Engineering Geology 294 (2021) 106345

Contents lists available at ScienceDirect

Engineering Geology

journal homepage: www.elsevier.com/locate/enggeo

Monitoring and analysis of the exceptional displacements affecting debris at the top of a highly disaggregated rockslide

Tommaso Carlà *, Giovanni Gigli, Luca Lombardi, Massimiliano Nocentini, Nicola Casagli

University of Florence, Department of Earth Sciences, Via La Pira 4, 50121 Florence, Italy

ARTICLE INFO

Keywords:
Rockslides
Translational rock–debris slides
GBInSAR
Balanced cross-section
FEM

ABSTRACT

The activity of large rockslides is dependent on a combination of interplaying factors that control strain localization within the slope. In some cases, continued deformation may lead to widespread disaggregation of the slide mass (i.e., loss of cohesion and development of debris). Layers with markedly different composition and strength may eventually form, making it difficult to assess the actual nature of hazards and related risks posed to the valley bottom. This paper provides updated insights into the highly disaggregated and rapidly evolving Ruinon rockslide (Central Italian Alps) based on more than a decade of monitoring by means of a Ground-Based Interferometric Synthetic Aperture Radar (GBInSAR). The rockslide was recently affected by a prolonged period of exceptional surface velocities—consistently exceeding 1 m/day. Monitoring data are examined in order to estimate the thickness of the rapidly moving layer of upper chaotic debris by means of the balanced cross-section method as well as determine the effects of hydrological forcing on the slope displacements. Finite-element modelling is then used to derive hypotheses concerning the deformation behavior of the slide mass at greater depth and different elevations. It is suggested that the upper debris moves at rates several orders of magnitude higher than the underlying substrate, and that in relative terms the sensitivity to sliding of the two layers is similarly governed by the increase of piezometric levels in the spring/summer. On lower slopes, the activity of the upper debris appears to be also influenced by precipitation events that are not accompanied by a notable increase of the piezometric levels measured at the rear of the slide. Our findings show the importance of implementing long-term GBInSAR monitoring at challenging sites like Ruinon, where fieldwork and installation of instruments on the slide mass are not feasible.

1. Introduction

The development of large rockslides in high alpine slopes implies complex processes of rock damage accumulation taking place under subcritical stress conditions. These stresses are sufficient to produce permanent deformation but are too small to generate sudden movement and collapse, though they may still contribute towards long-term progressive failure of the slope. While large rockslides slowly creep (i.e., deform more or less continuously under gravity and external loading; Emery, 1979; Hungr et al., 2014) with seemingly no risk posed to the valley bottom, rapid stress changes due to pore water pressure perturbations can produce strain localization and dramatic increments of velocity (Preisig et al., 2016; Vallet et al., 2016; Agliardi et al., 2020). In the worst-case scenario, an acceleration pulse is the precursor to runaway rupture and partial or total catastrophic collapse of the slope, which induces the formation of a rock avalanche. However, phases of accelerating displacements are most of the times episodic, and activity later returns to background levels (Hungr et al., 2005; Bonzanigo et al., 2007; Eberhardt, 2008; Crosta et al., 2014; Preisig, 2020). Such stick-slip behavior has been related to shear zone dilatant strengthening promoted by undrained hydro-mechanical coupling (Iverson, 2005; Schulz et al., 2009; Agliardi et al., 2020). Further hindering predictive and modelling abilities, time-dependent strength deterioration may determine a response to hydrological forcing that is not univocal over time and slope location, especially if the slide mass consists of an assemblage of different or variably altered materials. Since sub-surface data are rarely continuous over long periods, or may not be collected at all in rockslides affected by intense deformation, it follows that hazard assessment vastly relies on monitoring the surface displacements. A proper understanding of what these may represent in terms of the overall slope dynamics is necessary to reduce incorrect alarms. Recent examples of rockslide characterization through the analysis of surface

* Corresponding author.
E-mail address: tommaso.carla@unifi.it (T. Carlà).

https://doi.org/10.1016/j.enggeo.2021.106345
Received 14 September 2020; Received in revised form 20 August 2021; Accepted 24 August 2021
Available online 30 August 2021

displacement data are provided in Bonzanigo et al. (2007), Barla et al. (2010), Crosta et al. (2014), Palis et al. (2017), and Zangerl et al. (2019).

Establishing objective early-warning criteria based on judgmental approach and comparison with precedents is nonetheless problematic, as many large rockslides can be associated with a unique set of distinctive deformation styles and velocities. Some undergo sudden, short-lived accelerations and attain maximum velocities in the order of few millimeters per day. Others have a more ductile nature, meaning that they are able to accommodate much higher velocities (up to tens of centimeters per day) for longer periods (Hungr et al., 2005; Preisig et al., 2016). The delay between hydrological input and slope response, being subject to the local complexity of the underground flow regime, can also be of substantially diverse length. Slopes in strongly anisotropic metamorphic rocks tend to have a pronounced activity, propelling extensive shallow disaggregation of the slide mass and production of incoherent material (Glastonbury and Fell, 2008). This upper layer of debris may become sufficiently thick and widespread to attain a deformation behavior that is considerably different from that of the underlying substrate (the word "debris" here complies with the commonly used meaning given by Hungr et al., 2014).

Reliable quantitative analysis of superficial slope movements is strictly dependent on the spatial and temporal sampling of the collected measurements. In addition, monitoring should be performed for long enough so to allow observation of multiple reactivation events and how these relate to each other. The more detailed the monitoring data, the more the possibilities of establishing basic conceptual models and individuating the main factors that destabilize the slope. Ground-Based Interferometric Synthetic Aperture Radar (GBInSAR) is probably the reference standard for fulfilling the task of comprehensive slope monitoring thanks to an unmatched combination of accuracy, spatio-temporal resolution, remote sensing capability, and field of view extent (Antonello et al., 2004; Luzi et al., 2004; Barla et al., 2010; Casagli et al., 2010; Monserrat et al., 2014; Atzeni et al., 2015; Caduff et al., 2015; Carlà et al., 2019; Pieraccini and Miccinesi, 2019; Woods et al., 2020). The technique is suited to detecting velocities ranging from few centimeters per year to about 2–3 m/day, encompassing the full spectrum displayed by large rockslides (Barla et al., 2017).

This paper presents the outcomes of more than a decade of GBInSAR monitoring at the Ruinon rockslide, a highly disaggregated translational slide in phyllites and blocky/chaotic debris which has been recently affected by recurrent reactivations. In particular, the reactivation event that started in June 2019 coincided with a remarkable change of deformation behavior compared to previous years: surface velocities locally increased to more than 1 m/day, and maintained similar values for the successive 5 months. Against perceived expectations of local authorities, no sudden movement and large-scale collapse of the slide mass occurred. The GBInSAR dataset is reviewed to get an updated understanding of: the maximum thickness of the upper debris affected by greater deformation; how hydrological forcing drove the recent rockslide reactivations; and how deformation is distributed at different elevations and depths. To these aims, displacement data are exploited for application of the balanced cross-section method; representative trends of displacement/velocity from different slope sectors are evaluated against piezometric, rainfall, and snow depth measurements collected outside the slide boundaries; and a finite-element model is created from the inferred geometry and average strength/elastic properties of the slope materials. Even though the tendency to instability seems extremely variable in space, depth, and time, the analysis reveals common treats with regards to relative deformation behavior and susceptibility to hydrological forcing across the rockslide area.

2. General setting of the Ruinon rockslide

The Ruinon rockslide is one of the most active landslides in the alpine arc. It is located in the Upper Valtellina (Central Italian Alps), on the right flank of the steep valley of glacial origin incised by the Frodolfo River (Fig. 1). The slide mass is believed to extend down to a depth of approximately 50–70 m (Crosta and Agliardi, 2003; Crosta et al., 2017), for a total estimated volume of ~30 million m^3. Pre-Permian phyllites belonging to the Austroalpine Campo Nappe are the predominant lithotype in the area, with some interbedded layers of isoclinally folded marbles and metabasites. The rockslide is located at the base of a deep-seated gravitational slope deformation, which affects the entire slope up to its summit at 3000 m a.s.l. In this regard, Agliardi et al. (2001) documented the presence of geomorphological indicators like double ridges, graben-like depressions, trenches, scarps, and counterscarps. Paraglacial stress release and WNW-ESE trending fractures have been invoked as the main predisposing factors to slope instability (Agliardi et al., 2001).

The characteristics of the Ruinon rockslide adhere well to the description of what Glastonbury and Fell (2008) term "translational rock–debris slides", a class of rockslides composed of a mixture of debris and heavily fractured rock. In these phenomena, the marked tendency for disaggregation of the slide mass may give rise to the simultaneous, more or less interdependent deformation and sliding of different layers of rock and debris. They originate through progressive deepening and rearward extension related to rapid fluvial downcutting of slopes in strongly anisotropic lithotypes.

The Ruinon rockslide extends at elevations between 1600 and 2100 m a.s.l. and is characterized by two major scarps (Fig. 2a–b). The so called upper scarp identifies the active slide head and corresponds to a sub-vertical rock cliff of about 30 m in height. Here the outcropping rock mass is heavily fractured and intersected by a dense network of tension cracks, which favor its breakdown through small-scale planar and toppling failures. These induced the accumulation of a layer of blocky debris at its base, which further downslope is bordered by a forested area. The lower scarp (1900 m a.s.l.) is sub-parallel to the upper scarp and cuts through both soil and the rock mass. Starting from the early 2000s, the lower scarp experienced multiple retrogression phases and variations of planimetric geometry. This, combined with in-situ rock degradation, internal shearing of the slide mass, and incorporation of previously intact ground, contributed to the production of a more widespread debris cover, consisting of highly disoriented phyllite boulders in an abundant silty–clayey matrix ("chaotic debris"). The size of phyllite boulders ranges from that of gravel to more than 10 m in diameter. Over the years, a large lobe of chaotic debris—corresponding to an area that recently experienced rapid acceleration ("highly active debris slide" in Fig. 2)—has propagated towards the valley bottom, with the superimposition of secondary mass wasting processes in the form of rockfalls, debris flows, and shallow slumps. Greater disaggregation and development of fine-grained matrix are observed from slide head towards the lower slopes (i.e., blocky to chaotic debris). The rockslide area is delimited on its lower right (NW) margin by another sub-vertical cliff, which has not shown relevant activity in recent times (Fig. 2a–b). The distribution of scarps and minor trenches behind the upper scarp, up to an elevation of more than 2300 m a.s.l. (Fig. 1), indicate that the region where deformation is currently concentrated could expand upslope (Crosta and Agliardi, 2003).

It has been recognized that pore water pressures likely influence the activity of Ruinon (Del Ventisette et al., 2012), though it is not clear what is the relative contribution of rainfall infiltration and deep groundwater recharge. Reactivations have primarily occurred in late spring or early summer. Numerous springs are counted within and in the surroundings of the rockslide boundaries (Fig. 1); some of them give place to ephemeral flows that infiltrate again just beyond their point of emergence. Attempts at reconstructing the underground flow regime through discharge and chemical monitoring of the springs have been so far inconclusive, thus suggesting that these are fed by a deep groundwater system. In this sense, a prominent role is presumably played by the Confinale Creek, which borders most of the left flank of the rockslide (Figs. 1 and 2) and suffers from considerable losses of discharge between 2300 m a.s.l. (in proximity of the NE margin of the upper scarp) and the

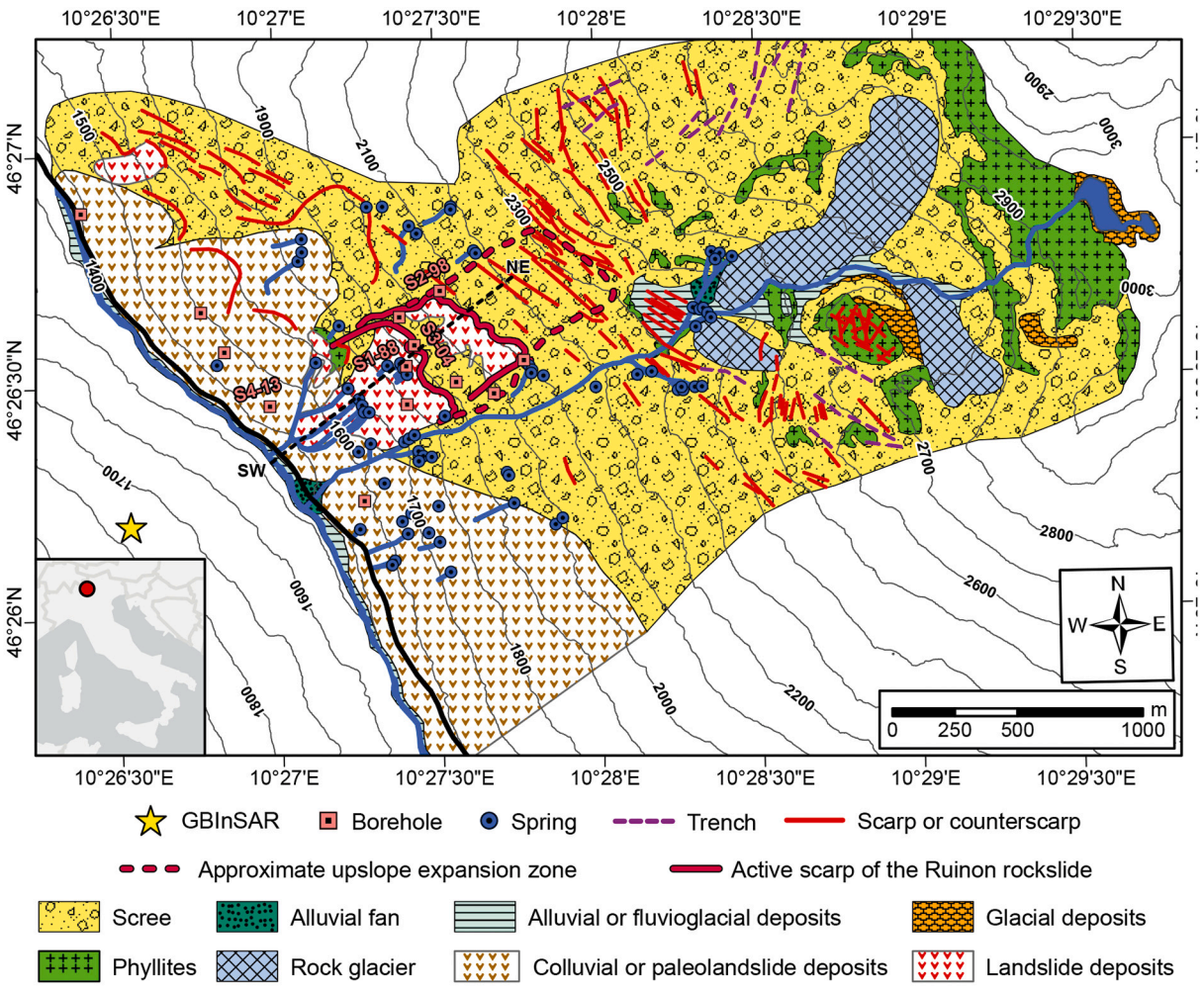

Fig. 1. Map of the Frodolfo River valley illustrating the main lithological units and geomorphological features in the study area.

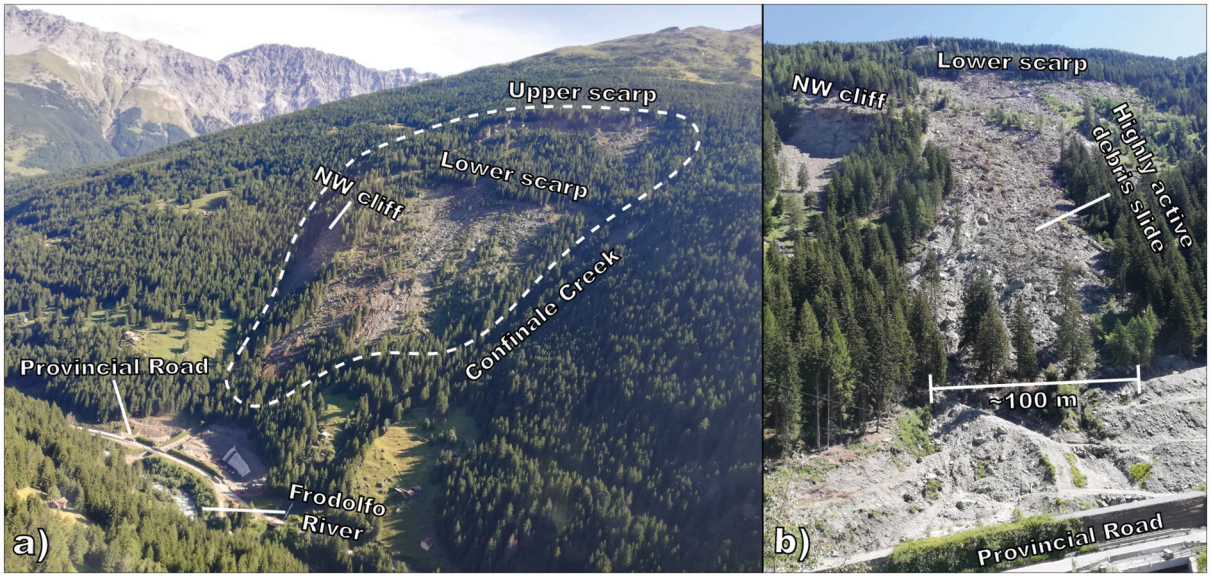

Fig. 2. Aerial photo of the Ruinon rockslide looking North (a) and frontal view of the lobe of rapidly sliding chaotic debris (b). The white dashed line approximates the external boundaries of the rockslide area.

confluence with the Frodolfo River. Losses of more than 80% over an initial average discharge of approximately 100 l/s have been estimated through installation of six V-notch weirs along the stream bed (G. Merizzi, personal communication, September 2019).

Slope hazards related to the evolution of the Ruinon rockslide seriously impacted a provincial road that travels through the valley bottom and connects the town of Bormio to other renown localities in the Upper Valtellina. There are multiple historical accounts of rockfalls and small debris flows temporarily blocking the road and causing the isolation of the village of Santa Caterina, located at the southeastern end of the valley. At the beginning of the seasonal reactivations between April–July 2014 and 2016, accelerated displacements led to short intervals of road closure in anticipation of a possible progression of the slide mass downslope of the lower scarp towards sudden movement and collapse. The same scenario repeated itself more alarmingly in June 2019: velocities increased to much larger values than ever recorded before—reaching more than 1 m/day—and remained constant for more than 5 months, even during subsequent phases of dry weather and until arrival of the winter season. Although a failure of the rockslide still did not occur, a block of about 90 m^3 was released from the debris near the lower scarp and rolled/bounced down to the valley bottom, damaging the road and forcing its prolonged closure.

3. Summary of previous analyses and site investigations

For more than a decade, monitoring and early-warning at the Ruinon rockslide have been centered around a GBInSAR system permanently installed on the opposite side of the Frodolfo River valley at an elevation of 1800 m a.s.l. (Casagli et al., 2010; Del Ventisette et al., 2012; Crosta et al., 2017). The distance between the sensor and the rockslide spans from about 1 km over the lower slopes to about 1.6 km over the upper scarp (Fig. 1). The transceiver unit consists of a continuous-wave step-frequency radar operating in Ku band (central frequency ~ 17 GHz) and is moved by a motorized sled along a linear rail in order to create a synthetic aperture. The output signal is amplified and transmitted by two antennas that are also equipped for receiving the backscattered signal, making it possible to attain the distance (range) and direction (azimuth) of sufficiently coherent targets (i.e., pixels) within the illuminated scenario. In principle, line-of-sight (LOS) displacements of each pixel are calculated with sub-millimetric accuracy by exploiting the phase difference of the back-scattered signal between two or more coherent acquisitions, and by assessing the contribution that actually stems from the ground movement (Casagli et al., 2010). In the employed configuration, the spatial resolution of the created displacement maps is about 1.5 × 4.9 m at the farther point of the upper scarp. The scan time of image acquisition is manually changed from a minimum of 2 min when displacements accelerate to a maximum of 3 h when the rockslide moves at velocities of few millimeters per month during the winter. A shorter time span serves to avoid issues of phase ambiguity. These give place to homogeneous patterns of phase cycles (i.e., interferometric fringes), and arise when movements during an acquisition step exceed half a wavelength (~8.8 mm). A thorough description of the technique is beyond the scope of this paper and can be found in Antonello et al. (2004), Luzi et al. (2004), Monserrat et al. (2014), and Pieraccini and Miccinesi (2019).

Given the potential impact of a failure on nearby communities, other studies have already dealt more or less directly with various aspects of the Ruinon rockslide. Agliardi et al. (2001) developed a conceptual model of the kinematics, age, and state of activity of the DSGSD that incorporates Ruinon. Crosta and Agliardi (2003) proposed a generalized method to calculate alert velocity thresholds for active rockslides based on data locally acquired by laser distance measuring instruments and wire extensometers. The site was also picked for one of the first experimental applications of the GBInSAR technique to the monitoring of large slope instabilities (Tarchi et al., 2003; Casagli et al., 2010). GBInSAR data from years 2006–2007 were exploited by Del Ventisette et al. (2012) to outline the interdependence between displacements and rainfall. Finally, Crosta et al. (2017) described a similar analysis of rainfall intensity/duration and GBInSAR-derived displacements from years 2006–2014, after which a subdivision of the Ruinon rockslide into homogeneous domains with specific warning criteria was proposed.

These studies were supported by several site investigation campaigns performed prior to the first major reactivation of the rockslide in 2014. Worth to be mentioned are a series of borehole cores drilled within and near the active slide boundaries between years 1988–2013. Investigations also included seismic refraction surveys, geomechanical surveys, and geotechnical laboratory testing (e.g., uniaxial compression, direct shear tests), in order to retrieve elastic and strength properties of the materials (Infrastrutture Lombarde, 2013). More recently, fieldwork and installation of instruments on the slide mass have been impeded by safety and technical concerns related to the large slope displacements. Borehole logs drilled within the rockslide area helped infer the diagrammatic cross-section in Fig. 3 (adapted from Crosta et al., 2017). This shows a variably thick layer of blocky/chaotic debris (broadly quantified between 10 and 30 m) overlying variably fractured/disturbed phyllites, but it should be noted that the transition from the upper debris to the disturbed phyllites is not as sharp as schematically illustrated. The same applies to the transition from disturbed to undisturbed phyllites. In general, the degree of disaggregation and rock mass damage gradually decrease with depth. Many uncertainties remain with regards to the subsurface pattern of deformation, since inclinometer casings have been historically sheared off quickly after installation due to the activity of the upper debris. The most compelling inclinometer records refer to borehole S1 (Fig. 1), where only two acquisition campaigns could be performed between 1988 and 1989. These measurements pointed at two shear surfaces near the base of the debris, at approximate depths of 15 m and 25 m (Fig. 3). The short monitoring period meant that slower movements involving the underlying substrate could not be assessed. Deeper shear zones of uncertain origin were correlated with the identification near the undisturbed substrate of up to 2-m thick layers of cataclastic granular material (e.g., boreholes S1–88 and S3–04), which are associated with a sudden drop of the RQD index towards zero and a highly weathered silty matrix (Agliardi et al., 2001). The presence of multiple weak layers was interpreted as a sign that significant internal differential movements could exist from slide base up to the surface.

Building upon the existing set of knowledge, newly updated GBInSAR, UAV-based (Unmanned Aerial Vehicle), rainfall, snow depth, and piezometric measurements are herein analyzed. UAV-based, snow depth, and piezometric measurements have not been explicitly considered in prior studies of the Ruinon rockslide. GBInSAR and rainfall measurements from years 2015–2019 (with special emphasis on the exceptional reactivation in 2019) are also addressed here for the first time.

4. Updated surface displacement data derived from GBInSAR and UAV monitoring

The rockslide area was divided into four sectors (Fig. 4) based on the following arguments:

- LSC (Lower Slope – Central): includes the central part of the lower scarp and the highly active mass of debris located downslope, which has been recently affected by exceptional displacements. This sector features hummocky ground in chaotic debris, a high degree of disaggregation, and generally greater development of silty matrix than elsewhere in the slope.
- LSLF (Lower Slope – Left Flank): corresponds to the area between LSC and the eastern boundary of the rockslide. Material composition and slope morphology in the two sectors are rather similar, with the main differences being the lower total displacements, the poorer development of silty matrix and a more extensive presence of vegetated terrain.

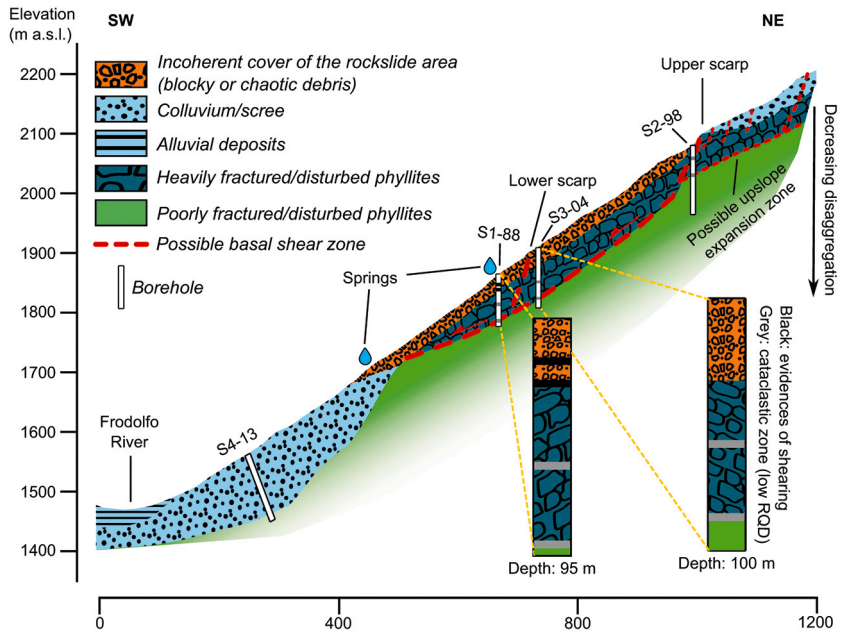

Fig. 3. Diagrammatic cross-section of the Ruinon rockslide (adapted from Crosta et al., 2017). Note that the figure does not capture the gradual transition from blocky/chaotic debris to disturbed phyllites, as well as the transition from disturbed to undisturbed phyllites.

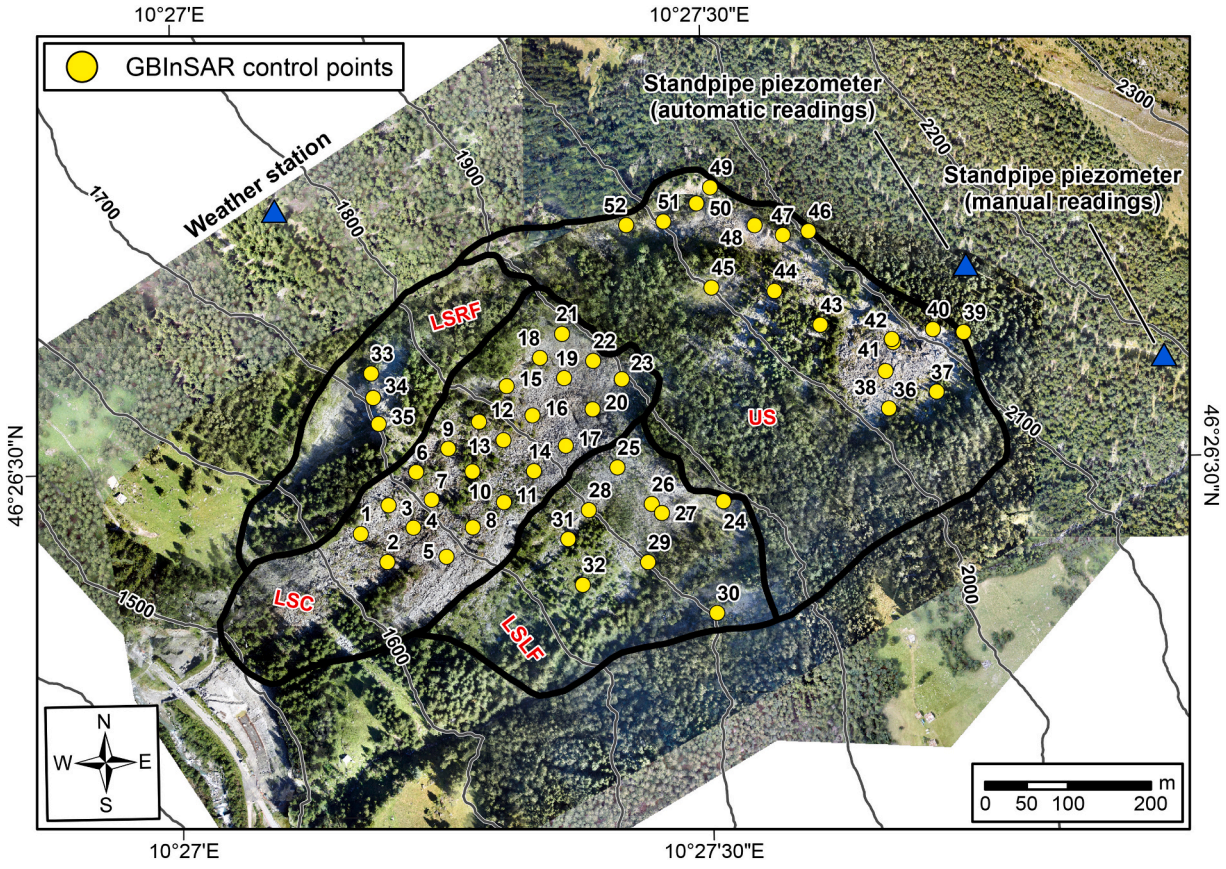

Fig. 4. Subdivision of the rockslide area into four main sectors (see text for explanation). Numbered yellow dots correspond to selected GBInSAR control points. (For interpretation of the references to color in this figure legend, the reader is referred to the web version of this article.)

- LSRF (Lower Slope – Right Flank): corresponds to the area between LSC and the western boundary of the rockslide. It includes the rock mass exposed by the NW cliff, the underlying colluvium originated from rockfalls, and the heavily forested terrain between the NW cliff and the lower scarp. Minor tension cracks sporadically cut the terrain behind the NW cliff.
- US (Upper Slope): delimits the area between the upper and lower scarps. Debris has a visibly blockier character than on lower slopes (i.

e., lower development of matrix), and mostly accumulates near the base of the upper scarp portions that have recently experienced instability and retrogressive activity. Areas characterized by low activity are generally forested.

A total of 52 GBInSAR control points—namely highly coherent pixels of the radar image—was selected to extract representative displacement/velocity time series of each of the listed sectors (Fig. 4). A comprehensive distribution of control points could be achieved only in LSC, that is where most of the vegetation has been cleared by the intense slope movements.

Fig. 5 highlights the annual cumulative displacements measured by the GBInSAR from 2009 to 2019 (i.e., for each year, displacement amounts refer to the interval from January 1 to December 31). It can be observed that displacements in the first 3 years of the dataset (i.e., 2009–2011) were relatively low and limited to small areas of LSLF and the left margin of US. Afterwards, intense deformation started to involve a large area covered by debris within LSC: here the seasonal reactivation that occurred in 2014 caused annual displacements to be for the first time in excess of 10 m, and to be diffusely in excess of 5 m. Similar data were collected in 2016, while the rest of the rockslide area did not suffer from evident variations of annual displacement up to 2018. A roughly 10-fold increase of the displacements was eventually observed in 2019, with maximum values of more than 150 m being detected near the lower margin of LSC. A noticeably higher deformation activity was also observed in proximity of the upper scarp and in LSRF, over the debris cover upslope of the NW cliff. Fig. 6 provides a closer look to the latest reactivation event, as displacements are in this instance cumulated on a monthly basis. It is shown that the debris slide in LSC followed an accelerating trend since the beginning of the year, while areas in US initially remained stable. Monthly displacements in both LSC and US then grew abruptly starting from June, and in the lower slopes remained consistently in excess of 10 m/month until November. A clear decelerating trend started only in December, concurrently with the first snowfalls of the winter (these are also responsible for the scattered movements erroneously measured across the entire radar map).

Fig. 7 provides a synoptic view of the GBInSAR dataset by plotting the complete displacement–time curves of selected control points (Fig. 4). The majority of the control points show a generally consistent activity, with phases of increasing cumulative displacements variably distributed over the different years (this is less visible in the LSC plots due to the stretched axis scale range resulting from the exceptional acceleration in 2019). On the other hand, the displacements of several points in the US sector (e.g., P40 and P48) appear to be more exclusively restricted to shorter periods in 2014, 2016, and 2019, with basically no displacements being recorded in other years.

The magnitude and persistence of the displacements detected in 2019 look extraordinarily high for the type of investigated phenomenon. In response to the increasing deformation activity, in the summer of 2016 one of the local authorities overseeing the monitoring and hazard management strategies at Ruinon (ARPA Lombardia) began to perform periodic UAV-based photogrammetric surveys of the rockslide area (L. Beretta, personal communication, November 2019). In particular, orthorectified aerial photos (resolution 6 × 6 cm) and raw terrain point clouds acquired on 28 July 2016, 4 September 2019, and 25 October 2019 were made available to the authors and exploited for validating the interferometric measurements. Visual inspection did not reveal obvious errors in the generation and georeferencing of such products, with the exception of some distortion over the NW margin of the upper scarp in the survey of 4 September 2019. Minor defects, if present, were considered negligible when compared to the magnitude of the observed slope displacements.

The orthorectified aerial photos acquired on 4 September 2019 and 25 October 2019 allowed tracking the planimetric offset of objects on the ground that were clearly recognizable by virtue of their shape and size, such as large boulders and dead tree logs. For example, Fig. 8 shows a block with a surface area of roughly 10 m^2 translating by about 12.5 m from the first to the second image (i.e., over a period of 51 days). A total of 50 objects experiencing a planimetric offset greater than 2 m was individuated on the highly active debris slide in LSC. Fig. 9 presents a comparison between the cumulative displacements measured from inspection of the aerial photos and those measured by the GBInSAR system during the mentioned time interval. Raster maps were created by means of inverse distance weighted interpolation, and all the UAV-based displacement vectors are also displayed (these are in scale with the bar at the top right corner of the figure). Vectors are less closely spaced towards the toe of the slope, where deposition of the material was concentrated—and therefore where objects laying at ground level were more likely to be buried. The two sets of results reveal a very similar pattern, despite the finer detail of the contours in the GBInSAR map thanks to the much higher number of interpolated data points (i.e., pixels). Displacements in both maps gradually increase from higher to lower elevation, and range from a minimum of about 2 m to more than 50 m. It is likewise interesting to note the common identification of a small sector with displacements in excess of 20 m in proximity of the upper limit of the interpolated area. Accordingly, it can be concluded that GBInSAR data are indeed able to accurately describe the surface displacements across the monitored scenario.

Morphological changes induced by the rockslide activity were quantified by comparing the raw terrain point clouds acquired on 28 July 2016 and 4 September 2019. Vertical subtraction between data points with corresponding horizontal coordinates (search tolerance 1 cm) evidenced lowering of the ground level between 2 and 4 m over wide areas covered by debris in the LSC sector, and up to peak values of over 6 m in a small area where the substrate was ultimately exposed at the surface in the late fall of 2019 (Fig. 10). Elevation increased by equivalent amounts in the vicinity of the valley bottom, thus indicating significant material transfer in the form of upslope depletion and downslope accumulation. Little information could be extracted over the area currently occupied by the distal edge of the highly active debris slide, which was covered by a dense forest prior to the latest reactivation (sparse vegetation was manually filtered from the point clouds). Lowering of the ground level between 1 and 2 m was also observed in areas covered by debris immediately below the upper scarp, confirming that intense deformation was not only confined to the lower slopes. No appreciable elevation changes were observed over the rocky outcrops forming the upper scarp and the NW cliff.

5. Thickness of the highly active debris slide

Estimating the thickness of the highly active debris slide sitting at the top of the Ruinon slide mass is of great importance for accurate hazard assessment, since its sudden movement and collapse would likely produce long-runout debris avalanches even without involvement of the underlying substrate. Borehole logs drilled in 1988 and 2004 (i.e., S1–88, S3–04, and neighboring boreholes drilled in proximity of the lower scarp in Fig. 1) indicated that the thickness of the debris could vary between 10 and 30 m, and inclinometer measurements highlighted possible shearing at or in close proximity of the rock–debris interface—a feature that would be in line with the description of translational rock–debris slides proposed by Glastonbury and Fell (2008). Such information may not accurately represent the present-day situation, owing to the limited amount of acquisition campaigns and the accelerated slope evolution that occurred since then. Additional site investigations are currently not feasible, as these would have to be carried out under precarious safety conditions and instrumentation would be quickly damaged.

Noncontact methods may thus be used to indirectly retrieve the shallower depth at which shearing occurs and provide updated estimates about the extent of debris that is more prone to instability. Existing noncontact methods to infer the slip depth of different landslide types have been recently reviewed by Jaboyedoff et al. (2020) and Meier et al.

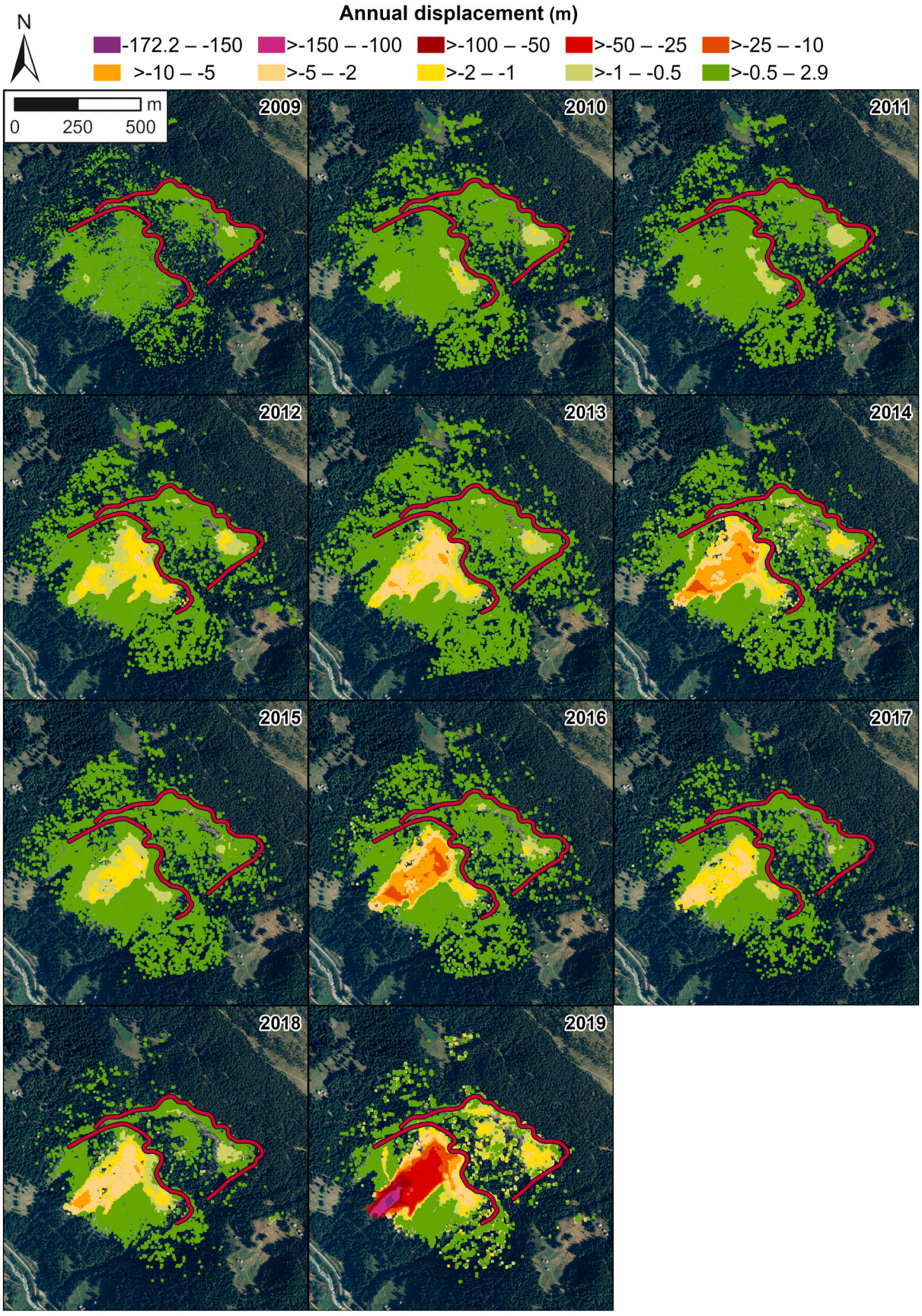

Fig. 5. Annual cumulative displacements measured by the GBInSAR system through years 2009–2019. Here and in the rest of the paper, displacements are intended as measured along the LOS, with negative values denoting movement towards the sensor and positive values movement away from the sensor.

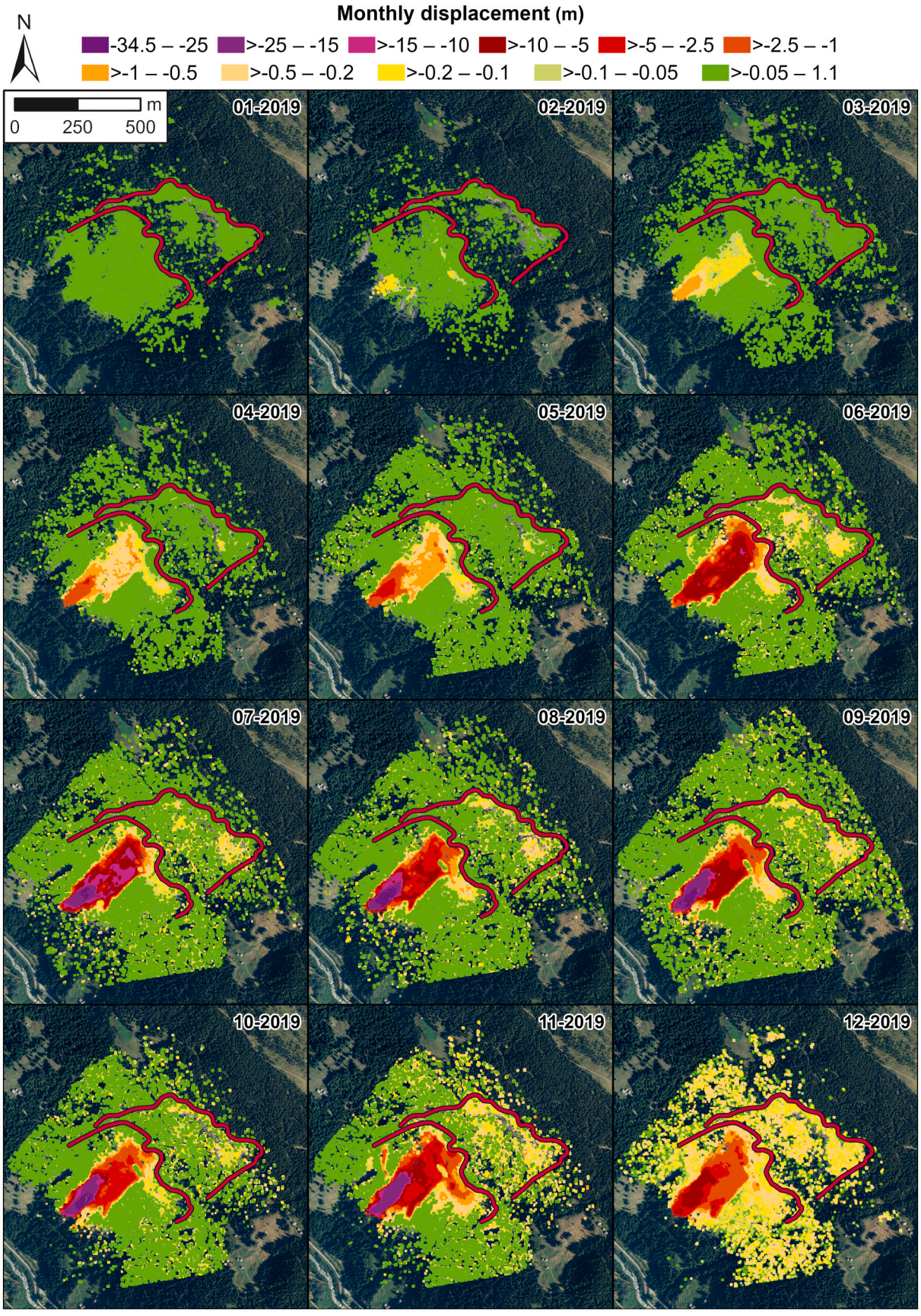

Fig. 6. Monthly cumulative displacements measured by the GBInSAR system from January to December 2019.

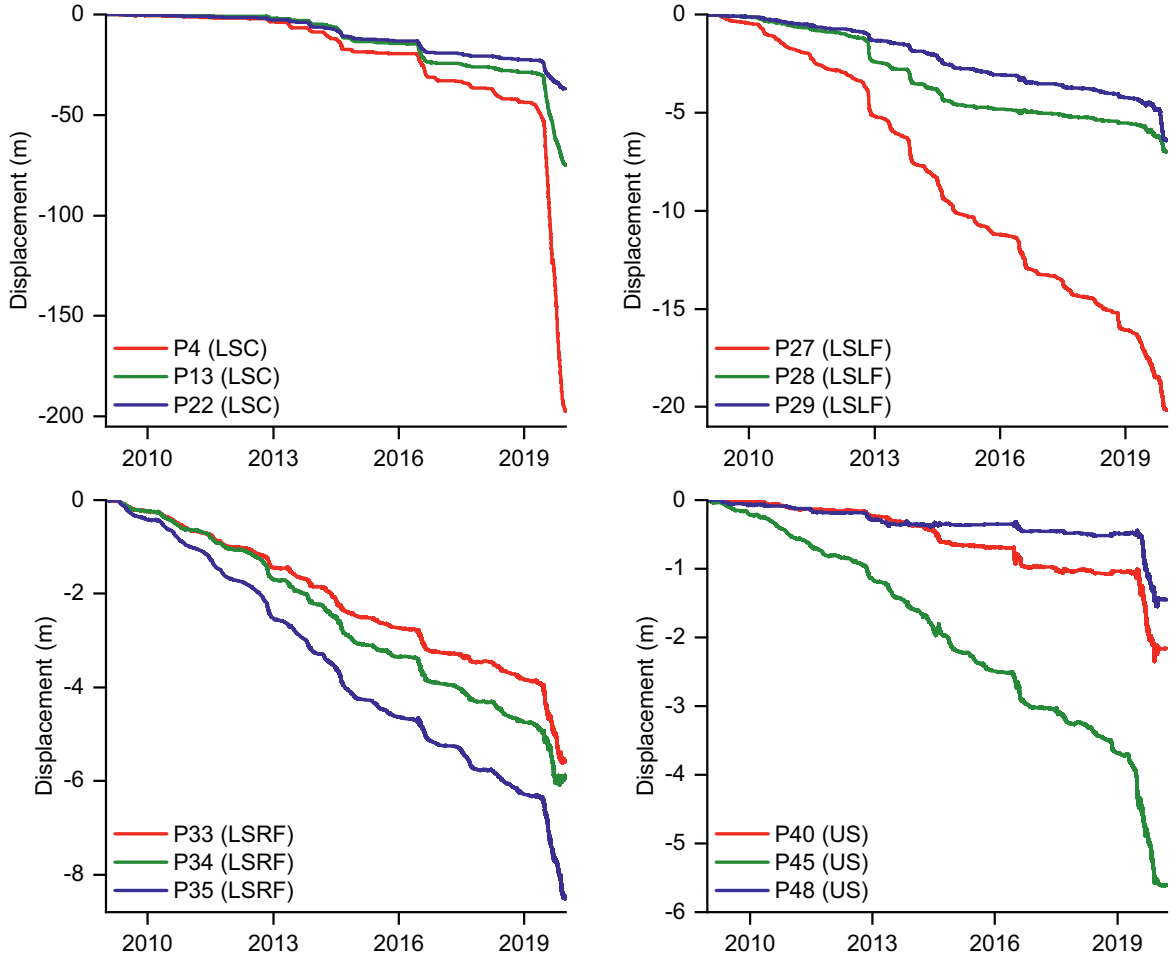

Fig. 7. Complete displacement–time curves of selected GBInSAR control points.

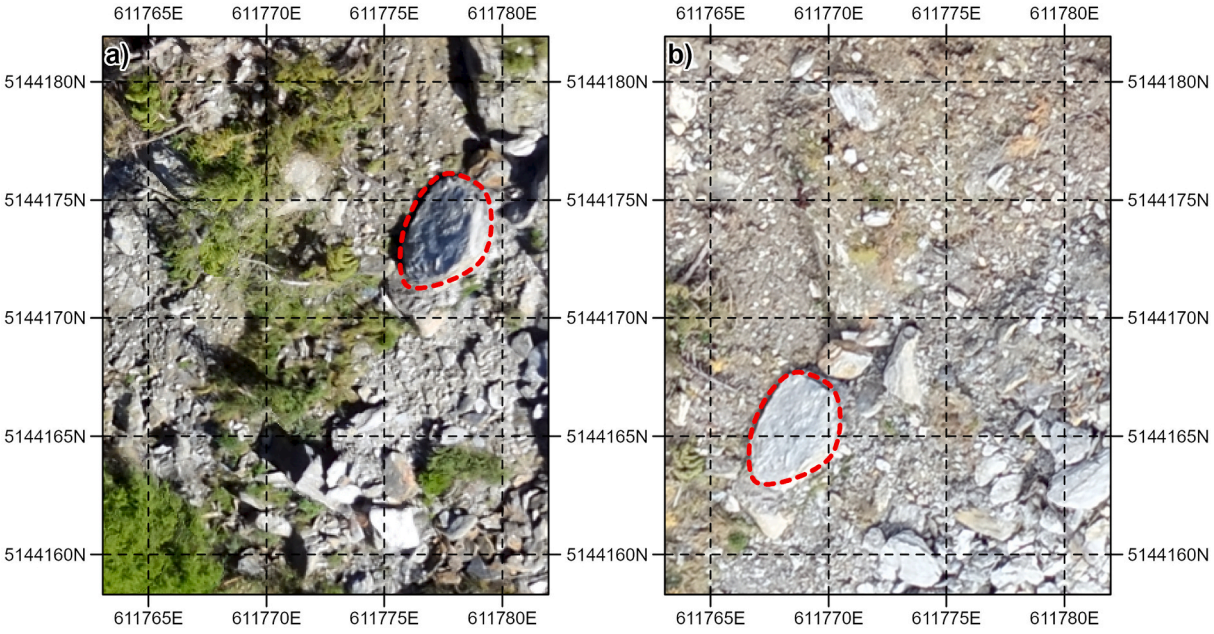

Fig. 8. Example of a large boulder translating by about 12.5 m in the period 4 September 2019 (a) – 25 October 2019 (b). Reference is made to the WGS 1984 UTM zone 32 N coordinate system.

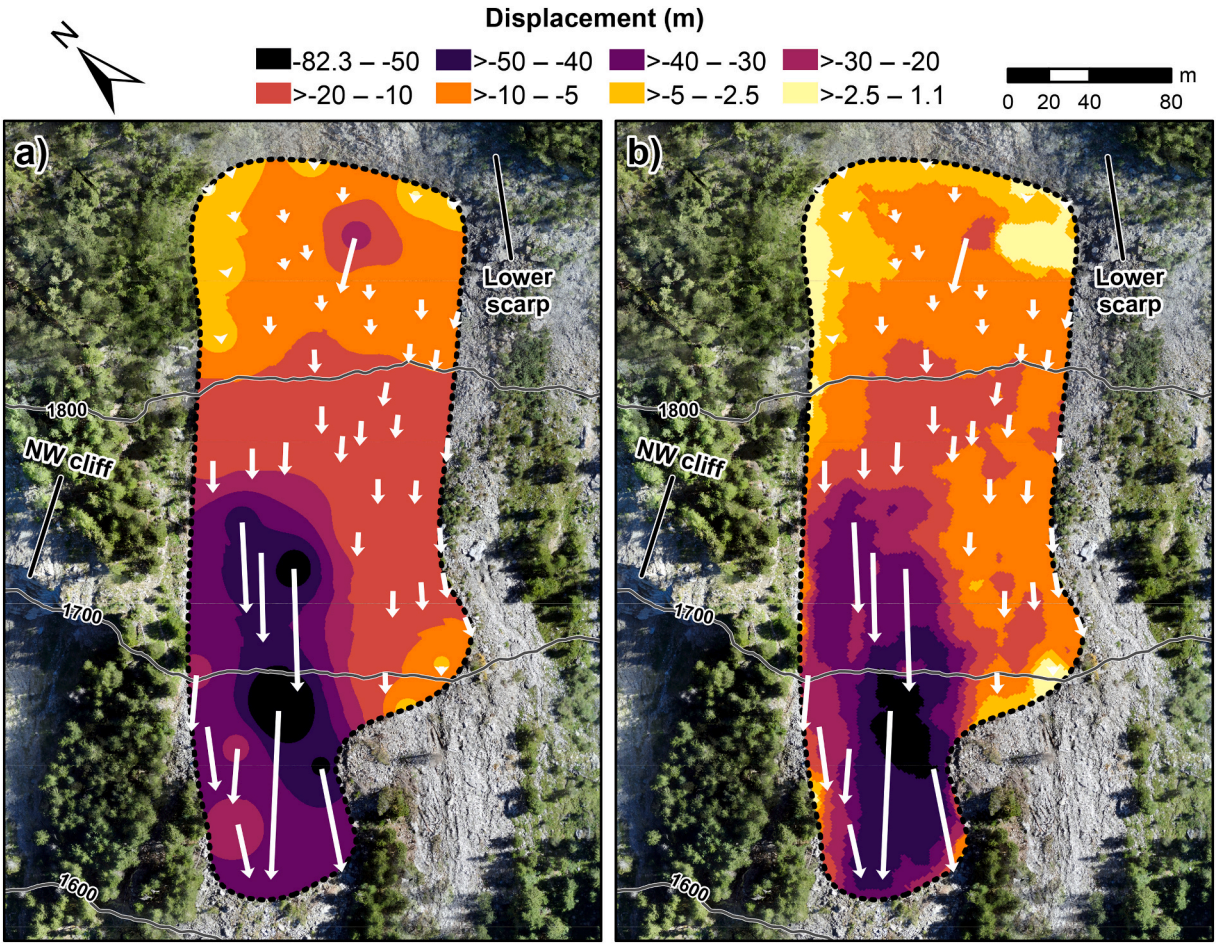

Fig. 9. Displacement maps derived from inspection of the UAV-based orthorectified aerial photos acquired on 4 September 2019 and 25 October 2019 (a), compared to the displacements measured by the GBInSAR system during the same period (b). The length of the vectors is consistent with the scale bar at the top right corner of the figure.

(2020). Among these, a versatile and yet relatively simple approach consists of geometrically balancing the area along a downslope cross-section, an approach also known as the Balanced Cross-section (BC) method (Hutchinson, 1983; Bishop, 1999; Aryal et al., 2015). The BC method is conceived for translational sliding movements: it considers plane strain, conservation of cross-sectional area, and no relevant bulking of the displaced material, so that movement can only occur in the downslope direction. Slip depth is calculated by dividing the area of the depletion zone at slide head by the mean displacement along the rest of the profile line towards slide base (Fig. 11A). The area of the depletion zone can be retrieved from expert judgement or comparison of pre- and post-failure terrain models, while the mean displacement downslope of the depletion area can be measured from surface observations (e.g., offset features) or surface monitoring.

A total of 10 transects were drawn across the LSC and LSLF sectors (Fig. 11B), where depletion zones were clearly recognizable and displacements were large enough not to constitute a relevant source of potential error (as opposed to the LSRF and US sectors). Relevant errors could rather stem from improperly processed terrain data or, alternatively, from violation of the model assumptions (Aryal et al., 2015), which in this case are not expected to be conspicuous given the markedly translating movement manifested by boulders at the surface (Figs. 8 and 9). The 28 July 2016 and 4 September 2019 photogrammetric surveys were considered as illustrative of the pre- and post-failure topography, and data acquired by the GBInSAR system during the same time interval were used for mean displacement calculation. A thickness value was assigned to each transect, hence allowing creation of a cross-slope slip surface profile (Fig. 11C). A null value was assumed at the NW end of the profile (i.e., lateral scarp at the right margin of LSC); from that point, the results imply that the base of the highly active debris slide drops quickly to a depth of approximately 18 m. This increases again farther to the SE and settles around a constant value of about 10 m. In this regard, it is reasonable that the rapidly moving layer of upper chaotic debris is thicker in the central part of the LSC sector, where the degree of disaggregation of the slide mass and the retrogression activity of the lower scarp are more pronounced. The results appear to agree well with observations made at borehole S1–88 (i.e., shearing at depths near the rock–debris interface), hence suggesting that most of the column of debris is affected by rapid sliding.

6. Impact of hydrological factors on slope displacements

Correlation between hydrological variables and slope displacements was performed using data from two standpipe piezometers and a weather station equipped with a non-heated tipping bucket rain gauge, respectively installed behind the upper scarp and 200 m westward of the NW cliff (Fig. 4). These data were collected by ARPA Lombardia as part of the monitoring and hazard management strategies implemented for the Ruinon rockslide (L. Dei Cas, personal communication, March 2020). Readings at one of the two standpipe piezometers have been carried out at irregular intervals since April 2012, while the second instrument was put into operation in June 2017 and equipped with a data logger for automatic piezometric monitoring at fixed intervals of 30 min. The boreholes containing the standpipe piezometers were drilled down

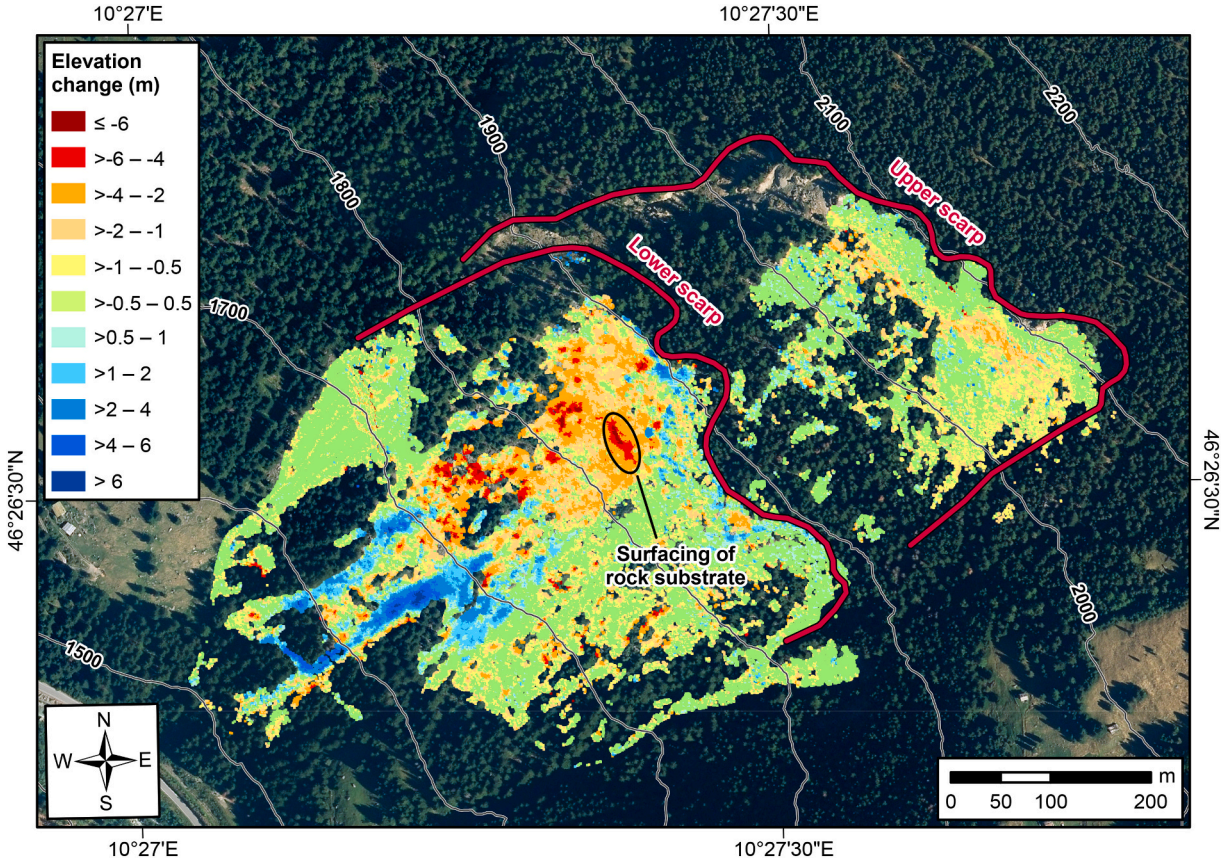

Fig. 10. Elevation change map obtained from comparison of the UAV-based photogrammetric surveys performed on 28 July 2016 and 4 September 2019.

to a depth of about 40 m, hence the tips are located near the rock–debris interface. Snow depth was measured by an ultrasonic snow depth sensor upslope of the area framed in Fig. 4 (elevation 2300 m a.s.l.).

Fig. 12 shows the variations of piezometric level with respect to the US and LSC velocities from 2014—year of the first major reactivation event—to 2019. In particular, velocities were obtained by averaging the measurements from every control point located in the respective sector (Fig. 4), and by filtering the resulting time series by means of a LOWESS (LOcally WEighted Scatterplot Smoothing) function. The rolling window of the LOWESS function was set to 90 data points, equivalent to a time length of roughly 3 h when the GBInSAR is pushed to its maximum acquisition frequency. This extensive filtering was applied in order to neglect short- and medium-term trend variations, and highlight only the long-term activity of the rockslide. It is observed that US and LSC velocities cyclically increase up to their maximum yearly value in late spring or early summer, and that maximum yearly velocities closely follow sharp peaks in values of piezometric level. Secondary accelerations occasionally happen in the fall, when heavy rainfalls determine small temporary reversals of the otherwise decreasing trend of piezometric level. Even though velocities at LSC are roughly one order of magnitude higher than at US, the two curves have a strikingly similar shape. This suggests that the tendency to instability in the two sectors is controlled by the same underlying mechanism. It is also worth noting that peak velocities during the reactivation event in 2019 were reached after the piezometric level rose to the maximum value ever recorded (~30 m below ground level). Fig. 13 further demonstrates the dependency of rockslide activity to hydrological forcing by outlining the correlation between the maximum velocity and the maximum piezometric level recorded each year during the spring/summer reactivations (automatic readings of piezometric level were picked over manual readings when both were available, since manual readings may suffer from censoring). The semi-log plot indicates that, as the height of the water table in proximity of the rockslide area grows, surface velocities increase in exponential fashion.

The effect of hydrological forcing on the slow-to-fast transitions of rockslide activity is also apparent when directly comparing surface displacements with precipitation data. Fig. 14 shows that the culmination of the reactivation event in 2019 took place at the end of the spring rainfalls—as highlighted by the continuous increase of the 90-day cumulated values up to the end of June—and a few weeks after the snow cover at higher elevation had completely melted. The same behavior exemplified in Fig. 14 applies to data from previous years as well.

The bubble plot in Fig. 15 summarizes how the intensity of the recent seasonal reactivations is well correlated with the precipitation amounts: the size of the data points is proportional to the average annual displacement of the LSC sector, while the blue tone is related to the sum of the normalized values of maximum snow depth recorded during the previous winter and 90-day cumulative rainfall at the time of reactivation onset. In other words, a normalized value of two would mean that the year was affected by the greatest rainfall and snow depth amounts in the entire dataset. It is evinced that: (i) the reactivation event in 2019 was characterized by the largest annual displacements and the most unfavorable weather conditions; (ii) data points of the other two principal reactivation events (2014 and 2016) are those that lie closer to the 2019 datum in terms of precipitation amounts; (iii) annual displacements were much lower when just a single precipitation variable was substantially below the 2019 amount (e.g., the reactivation event in 2017 took place in the aftermath of almost equal rainfall amounts than in 2019, but also of a substantially poorer snow accumulation).

7. Numerical modelling

Numerical techniques are a widely utilized tool for modelling and

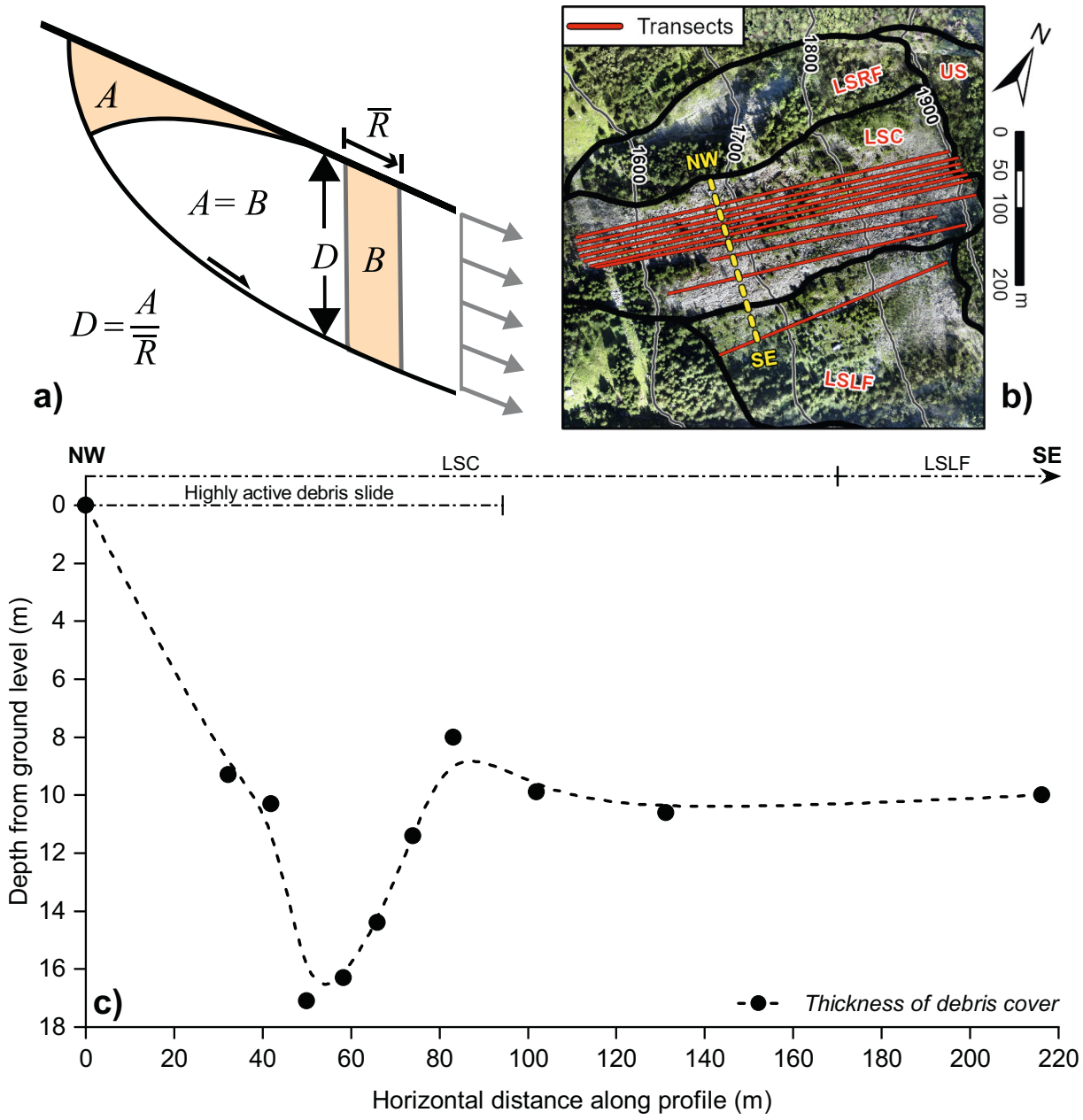

Fig. 11. (a) Conceptual scheme of the BC method (from Aryal et al., 2015); (b) transects used for application of the BC method; and (c) cross-slope slip surface profile expressing the thickness of the highly active debris slide located downslope of the lower scarp.

back-analyzing the stress/strain field within unstable slopes, as well as studying the influence of environmental factors in shifting the balance between driving and resisting forces. The finite-element method (FEM) considers the soil/rock mass as an equivalent continuum discretized into a set of sub-domains. The solution procedure exploits approximations to the connectivity of these sub-domains, and continuity of displacements and stresses between sub-domains (Eberhardt et al., 2004). Among other things, finite-element methods help reproduce important aspects related to landslide behavior such as failure mechanism and location, as concentrated groups of element transition from a condition of initial linear elastic state to one of plastic yield in response to the given problem geometry, gravity/in-situ stress fields, material properties, and predefined constitutive models. They also allow calculation of a FEM-based slope factor of safety through the shear strength reduction technique (Griffiths and Lane, 1999; Hungr et al., 2005; Eberhardt, 2008; Duncan et al., 2014).

A bi-dimensional model of the Ruinon slope was created by means of the commercial FEM code RS2 (Rocscience Inc., 2021). The aim was to back-analyze the conditions that lead to the rockslide reactivations and gain a better understanding of how slope deformation might be distributed with depth and at different elevations. The profile location, slope geometry, and subdivision into different material units are consistent with Fig. 3, meaning that a single upper layer of debris and a single underlying layer of disturbed phyllites were built into the model (with no joint boundaries). This simplification is justified by the absence of precise data constraining how disaggregation and material properties gradate with depth. Slight adjustments to the geometry of the rock–debris interface were made in accordance with: (i) the results obtained from application of the BC method for what concerns the thickness of the rapidly moving debris cover in the lower part of the LSC sector (maximum thickness ~ 18 m); (ii) the recent surfacing of rock substrate at an elevation of roughly 1850 m a.s.l (Fig. 10). Average strength and elastic properties of the debris and rock units retrieved during the 1988–2013 investigations are indicated in Tables 1 and 2. A small

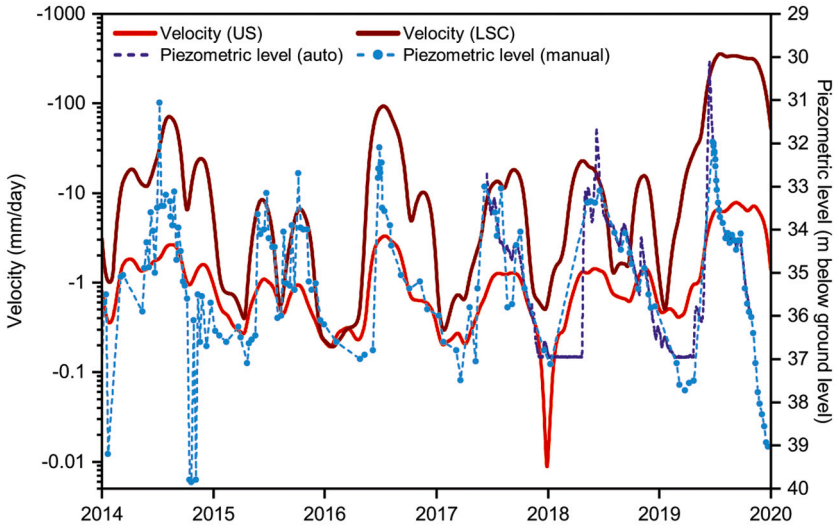

Fig. 12. Variations of piezometric level versus surface velocities of the US and LSC sectors from 2014 to 2019.

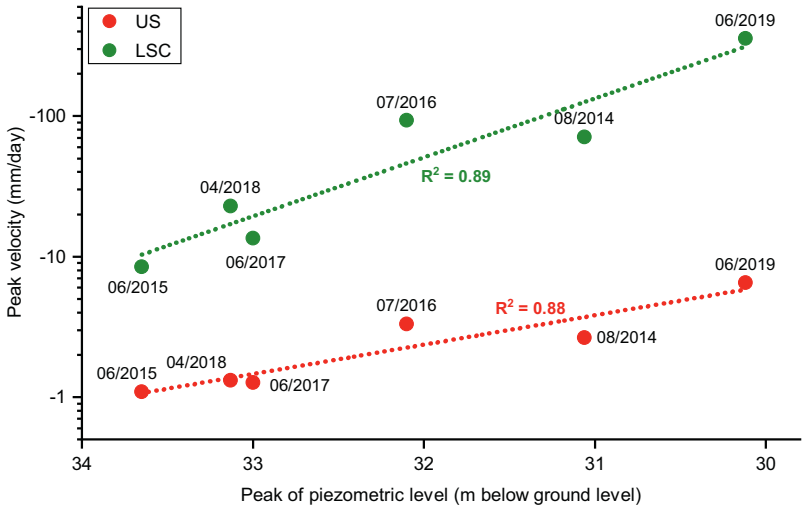

Fig. 13. Correlation between the peak surface velocities of the US and LSC sectors and the peak of piezometric level recorded each year at the rear of the slide during the spring/summer reactivation period.

cohesion component was applied to the debris through trial-and-error, in order to improve model convergence. Displacements along both axes were restrained at the base and sides of the model. The domain was discretized into a graded mesh of three-noded triangular finite elements.

The simulation was first run by considering all the materials as completely dry. This was made to assess the equilibrium of the slope without external forcing. A dry model can be considered descriptive of the winter season, when liquid precipitation is negligible and seepage is presumably inhibited by water freezing within fractures (as suggested by the intermittent character of springs within and in proximity of the rockslide area, which are typically inactive from November to April). Then, since no reliable information about the underground flow regime are available, a piezometric line was added to the model with the assumption of static water conditions. For the limitations stated above, the goal is not to reproduce the role played by seepage within the slope, but rather to infer whether the presence of significant pore pressures (as it occurs upon spring thawing) may lead to changes in the style of the slope deformation. The piezometric line was placed at a depth of 30 m below ground level behind the upper scarp, consistently with piezometric data collected in June 2019. The piezometric line was then raised in close proximity of the ground surface where new alignments of water springs were observed downslope of the lower scarp (see location of springs at an approximate elevation of 1700 and 1850 m in Fig. 1).

The results for the dry simulation, expressed in terms of the calculated total displacements (Fig. 16), reveal that the slope factor of safety almost equals unity. Deformation is exclusively shallow and is mostly concentrated downslope of the lower scarp, especially where the substrate is closer to the ground surface. In this phase nor the upper scarp area or the substrate seem to be affected by instability. For better visualization, the results for the simulation with the addition of a static water table are instead expressed in terms of the nodal deformation vectors (Fig. 17). Shear strains and total displacements of the upper debris increase by at least one order of magnitude and are accompanied by a decrease of the slope factor of safety well below unity, as convergence of the model starts to be lost when the strength reduction factor is ~0.75. Vectors throughout the debris show slightly variable directions and extend upslope to reach the location of the upper scarp, although deformation downslope of the lower scarp is still more intense. It is interesting to note that now also the disturbed rock mass is affected by very small movements, with deformation vectors that are sub-parallel to both the ground level and the interface with the undisturbed rock mass.

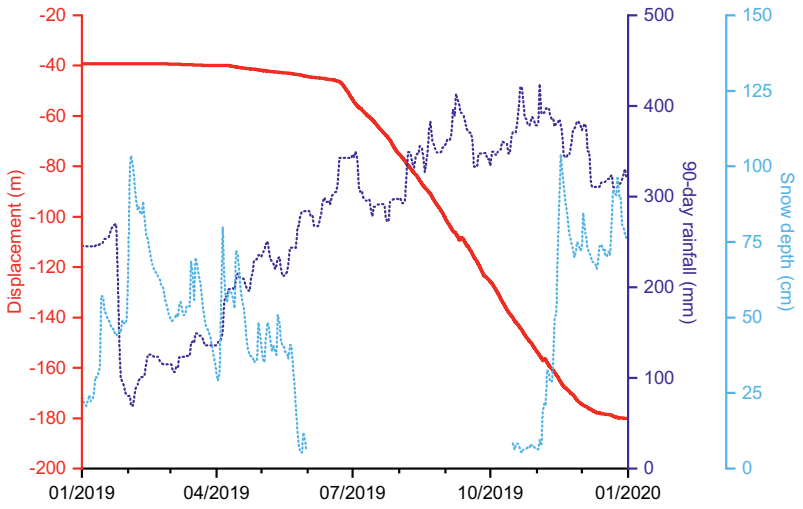

Fig. 14. Displacement–time curve of one of the GBInSAR pixels in the LSC sector versus values of 90-day cumulative rainfall and snow depth measured throughout 2019. Rainfall data are cumulated over 90 days so as to highlight the higher frequency of rainy days in the first half of the year.

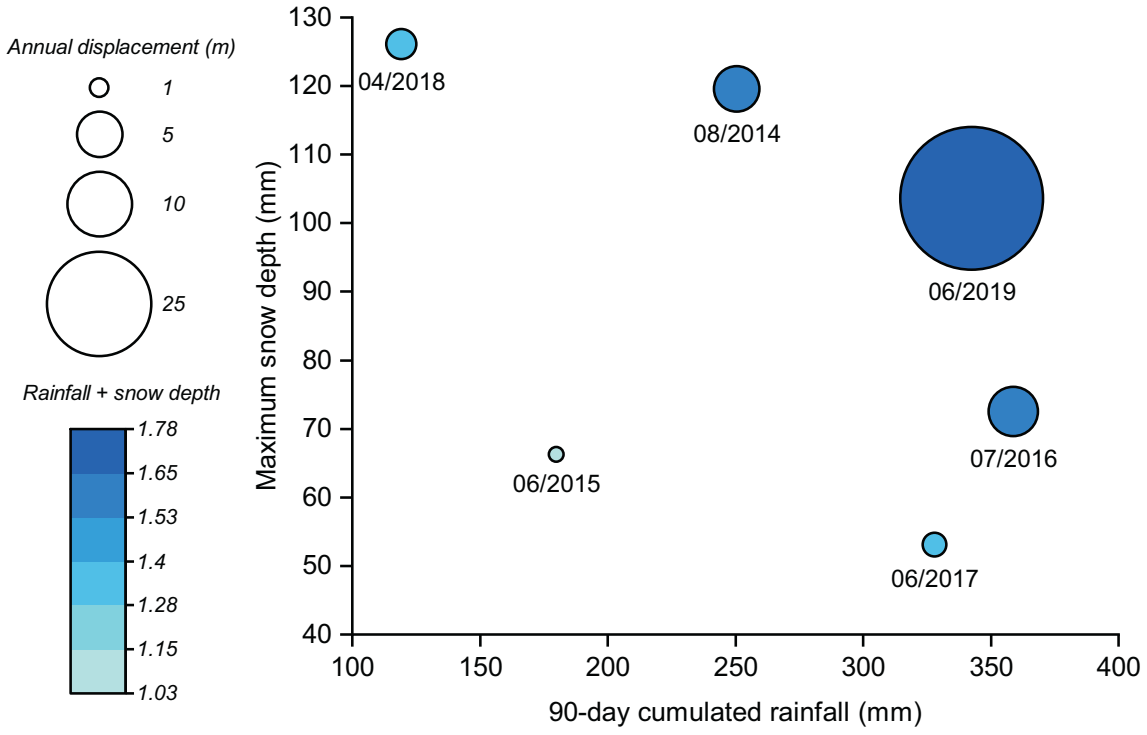

Fig. 15. Comparison of the conditions leading to the recent spring/summer reactivations of the Ruinon rockslide: 90-day cumulative rainfall at the time of the reactivation onset versus maximum snow depth recorded during the previous winter. Bubble size is proportional to the annual average displacement of the LSC sector.

Table 1
Soil unit properties used in the FEM simulations: γ = unit weight; ν = Poisson's ratio; E = Young's modulus; φ'_p = peak friction angle; c'_p = peak cohesion; φ'_r = residual friction angle; c'_r = residual cohesion; K_o = effective stress ratio.

Material	Failure criterion	γ (kN/m^3)	ν	E (MPa)	φ'_p (°)	c'_p (MPa)	φ'_r (°)	c'_r (MPa)	K_o
Debris cover of the rockslide area	Mohr-Coulomb	18.5	0.33	200	41	0.05	37	0.005	0.35
Colluvium/scree	Mohr Coulomb	20	0.33	400	43	0.05	37	0.01	0.35

Table 2
Rock unit properties used in the FEM simulations: γ = unit weight; ν = Poisson's ratio; E = Young's modulus; σ_{ci} = uniaxial compressive strength of the intact rock; m_b, s, and a = material constants for the intact rock; K_o = effective stress ratio.

Material	Failure criterion	γ (kN/m^3)	ν	E (MPa)	σ_{ci} (MPa)	m_b	s	a	K_o
Disturbed phyllites	Generalized Hoek-Brown	25	0.2	30,000	20	0.434	4.54×10^{-5}	0.585	0.25
Undisturbed phyllites	Generalized Hoek-Brown	25	0.2	30,000	48	1.077	0.001	0.516	0.25

8. Discussion

The Ruinon rockslide involves sectors of different material composition, morphology, and tendency to slope instability. In rockslides that are displaced along well-developed basal shear zones consisting of gouge layers, acceleration pulses may be precursors to a sudden reduction of shear strength followed by runaway rupture and catastrophic collapse (Agliardi et al., 2020). This kind of basal shear zone has not been conclusively identified at Ruinon. Moreover, the presence of a thick, highly disaggregated, and rapidly evolving debris cover over most of the rockslide area makes it challenging to understand the actual deformation behavior of the slide mass as a whole. Other than the large-scale collapse of the rockslide, possible event scenarios include rockfalls, debris flows, and—if considering the entire layer of chaotic debris below the lower scarp (LSC and LSLF sectors)—debris slides/avalanches of up to $>10^6$ m^3, all of which have substantial differences in terms of velocity, travel distance, and impact on the valley bottom. Performing realistic hazard assessment is made extremely problematic by the fact that the site has long been inaccessible due to the continuing large displacements, hence observational evidences may be complemented only with data collected from outside the slide boundaries. Some boreholes were drilled on the rockslide when this was at a much earlier stage of development, providing an incomplete picture about the distribution of materials and movements below ground level. This gives rise to significant uncertainties in the interpretation of the slope deformation behavior and evolution, especially with regards to the mechanism of the recent reactivations events that culminated into the exceptionally high velocities recorded in 2019. The implementation of long-term GBInSAR monitoring can thus become a critical tool by which such uncertainties may be at least partly reduced or constrained.

Due to the widespread presence of debris across the rockslide area, the phenomenon can also be regarded as a translational rock–debris slide according to the definition proposed by Glastonbury and Fell (2008), who describe this specific type of instabilities as being characterized by long histories of slow surface velocities (with reference to the landslide velocity classification of Cruden and Varnes, 1996) because the high permeability of the debris hinders abrupt rises of piezometric level. Still, velocities of the debris at Ruinon consistently surpassed 1 m/day, and data collected at the rear of the slide hint that abrupt rises of piezometric level can actually occur and influence its activity. No precise information about the hydrogeology of the slope is at this time available. Still, it can be postulated that groundwater flows converge around the rockslide area—to which the discharge losses of the Confinale Creek near the upper scarp may contribute decisively—and that seasonal snowmelt at high elevation promotes boosts of piezometric level in the spring/summer.

Variations of piezometric level have been recorded behind the upper scarp (thus outside the active slide boundaries), but can reasonably be expected to have occurred also in the materials located at close distance downslope. Figs. 12 and 13 demonstrate in fact that peaks of surface velocity correlate very well with peaks of piezometric level. Surface velocities—especially in the LSC sector—often seem to begin rising prior to the piezometric level, which could be explained by the local and superimposed response of the highly active debris slide to rainfall events antedating arrival of the lagged snowmelt input (Fig. 14). On the other hand, the results from the FEM simulations support the proposition that movements in the upper slopes are more exclusively triggered by high piezometric levels. This is in good agreement with data collected during the reactivation event in 2019, when areas belonging to the US sector began to accelerate later than areas belonging to the LSC and LSLF sectors (Fig. 6). More in detail, Fig. 18A compares the displacements of two control points during the period January–June 2019: one of the points (P16) is located within the LSC sector, the other (P42) in the US sector. Contrarily to P16, it can be seen that P42 undergoes a definite trend change only after the peak of piezometric level has been reached. It should be verified whether a similar response will recur in the future, since it may have significant implications for assessing the potential for instability in the upper scarp area and consequent rearward extension of the rockslide. It should also be mentioned that, other than in 2019, phases of displacement increase at several GBInSAR control points in the US sector were strictly limited to the reactivation events in 2014 and 2016 (Fig. 7). This is when the piezometric level measured at the rear of the slide rose to values not far from the 2019 peak (note that piezometric measurements in Fig. 12 may suffer from censoring before automatic monitoring was initiated in 2017).

While an explanation for the exceptional intensity of the reactivation event in 2019 may be sought in the general agreement between the magnitude of surface velocities and the seasonal peak of piezometric level at the rear of the slide, it is unclear why—differently to previous years—the high activity persisted for so long despite the continuous decrease of piezometric level after the end of June (Fig. 12). Relevant changes in shear stress with displacement may be excluded, owing to the prominent translational sliding mechanism of the upper debris (Fig. 8). The long-lived appearance of new spring alignments downslope of the lower scarp (see location of springs at an approximate elevation of 1700 and 1850 m in Fig. 1) may instead point to a more sustained continuity of high piezometric levels within this area of the rockslide with respect to the upper slopes.

Results from the FEM simulations also suggest that deformation in the upper scarp area may be associated with the activation of deeper movements in both the upper and lower sectors of the rockslide in the form of a much slower, mostly planar sliding of the underlying disturbed rock mass. Velocities are expected to increase from slide base up to the surface more gradually than what is shown in Fig. 17, given that the gradual disaggregation of the slide mass with depth cannot be properly modelled. Interpretation of the sub-surface deformation pattern is further complicated by the unknowns concerning the existence of preferential weak layers and the related possibility of complex internal differential movements.

The BC method provides an estimate of ~18 m for the slip depth of the highly active debris slide downslope of the lower scarp, corroborating the inclinometer measurements performed at borehole S1 in 1988–1989 and the idea that shearing occurs in close proximity of the rock–debris interface (Fig. 3). The upper debris is estimated to be in a state close to limit equilibrium regardless of the groundwater conditions (Fig. 16). Drops in the back-calculated factor of safety well below unity reflect the higher sensitivity of this material to pore water pressure buildups, which determine dramatic velocity increments. Secondary mass wasting processes induced by shallow deformation of the debris (i.e., rockfalls or shallow slumps) may thus be considered as always possible, and their probability enhanced during phases of high activity. It is stressed that the presented FEM models are meant to infer additional information about the possible slope deformation behavior on the basis of the limited available data and observational evidences. Actual values of the slope factor of safety will depend on the permeability of the materials within the slide mass and the detailed distribution of pressure

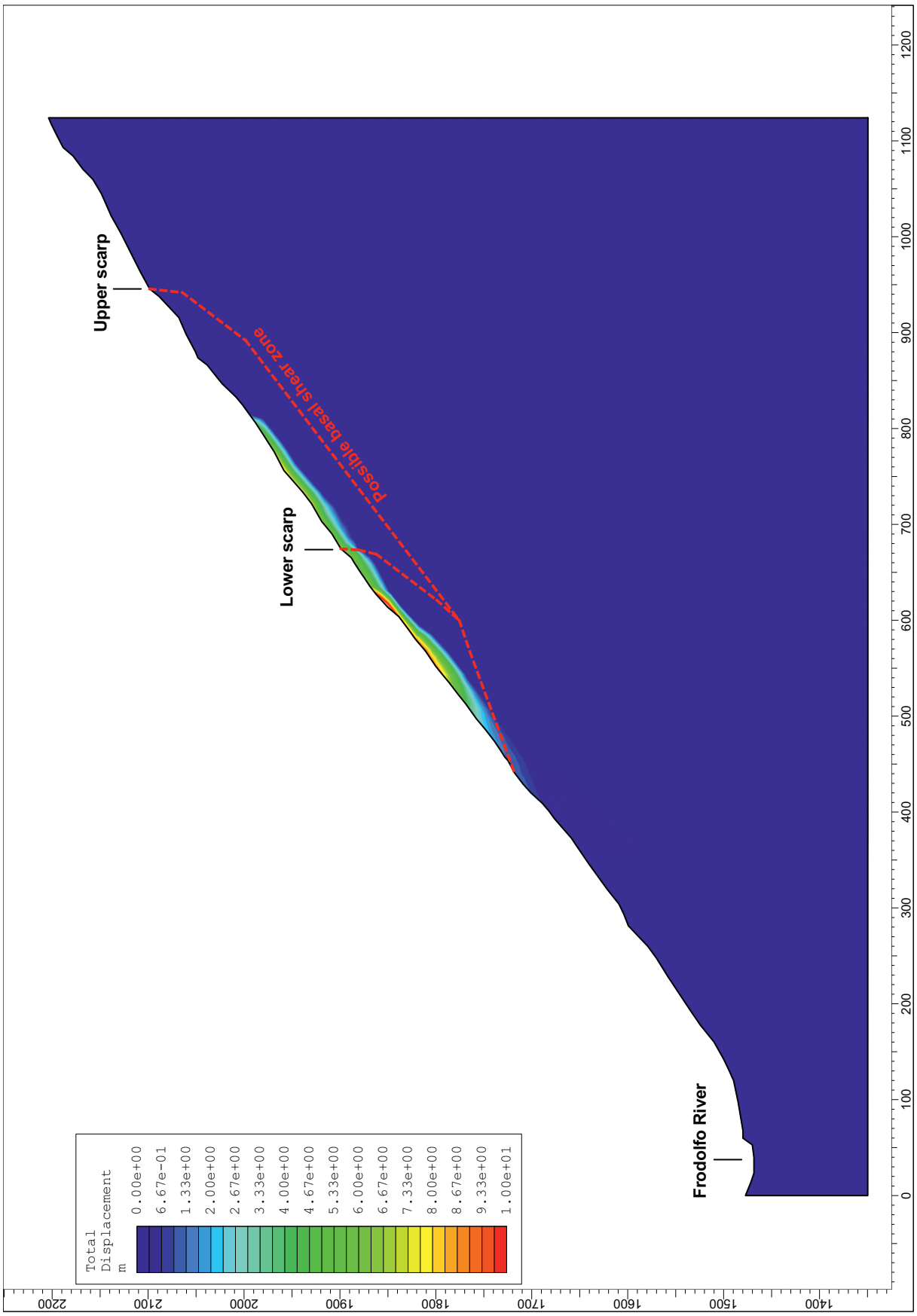

Fig. 16. Total displacements calculated for the dry RS2 model of the Ruinon slope. Model convergence is lost when the strength reduction factor approaches unity. The location of the possible basal shear zone within the substrate is indicated to provide visual reference with the diagrammatic cross-section in Fig. 3, however this does not imply the addition of an actual joint boundary into the model.

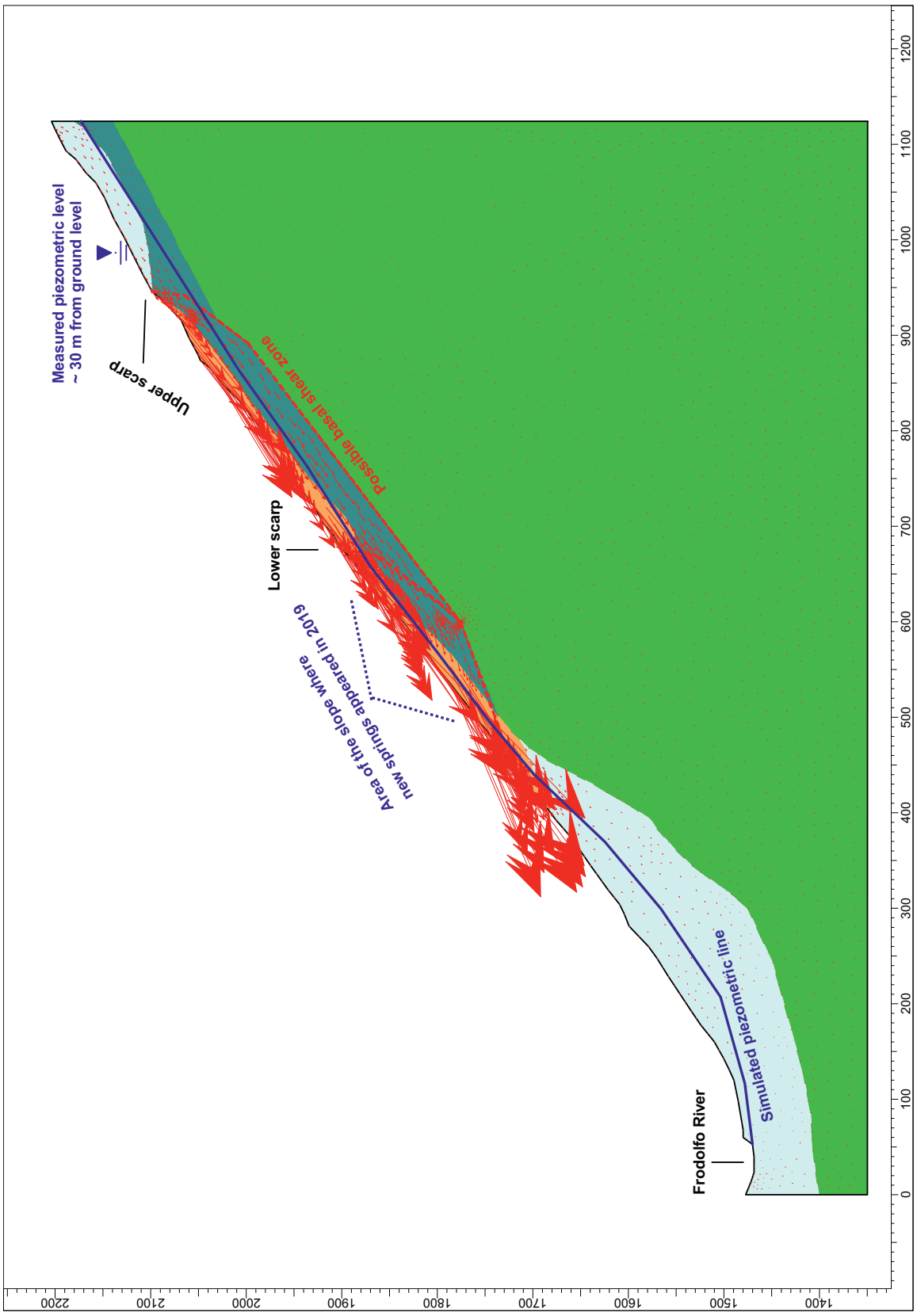

Fig. 17. Nodal deformation vectors for the RS2 model of the Ruinon slope, with addition of a static piezometric line. Model convergence is lost when the strength reduction factor is ~0.75. Color and meaning of the different material units are consistent with the diagrammatic cross-section in Fig. 3. The location of the possible basal shear zone within the substrate is indicated to provide visual reference with the mentioned figure, however this does not imply the addition of an actual joint boundary into the model.

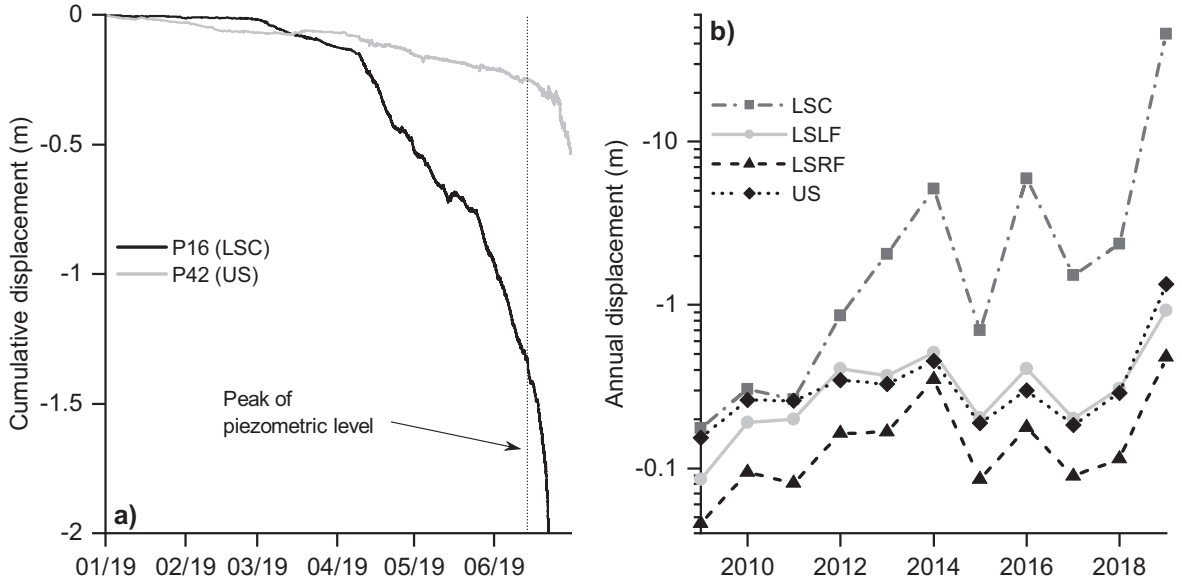

Fig. 18. Comparison between the displacements measured at control point P16 (LSC sector) and control point P42 (US sector) during the period January–June 2019 (a), and annual average displacements of each slope sector (b).

gradients, for which reliable measurements are again impossible to obtain at present.

Appraisal of the Ruinon evolution and related hazards should therefore take into account both the location and type of materials involved in the detected movements, together with a careful monitoring of the piezometric levels and rainfall amounts near the slide. Additional insights into the overall dynamics of the Ruinon rockslide are provided in Fig. 18B, which sets forth the displacements of the four slope sectors in logarithmic scale and cumulated on an annual basis. Annual displacements for each sector were calculated by averaging all the radar pixels enclosed by the respective boundaries. The line plots have remarkably comparable trends (especially since the first major reactivation in 2014), meaning that variations of annual displacement across the whole rockslide area have been proportionately similar over time. This again is an evidence that deformation at the surface, although manifesting itself under widely variable rates and modes, is for the most part triggered by the same underlying mechanism acting on the slope at large scale (i.e., groundwater recharge). In order to assess whether incipient conditions for the sudden movement and large-scale collapse of the Ruinon rockslide exist, progressive acceleration of localized portions of substrate would therefore represent a more meaningful precursory sign than the movements of the upper debris, irrespectively of how rapid and widespread these might be. In this sense, the small area of freshly outcropping substrate in the LSC sector (Fig. 10) has not shown appreciable displacements since being exposed by the rapid movements of the debris in late 2019. Within the external slide boundaries, other monitorable locations of outcropping substrate are only found discontinuously along the lower scarp; here, recent deformation activity has however been driven by local superficial retrogression of the scarp and may not be linked with the behavior of the substrate at depth.

9. Conclusions

The Ruinon rockslide is a large slope instability in a highly disaggregated mixture of phyllites and blocky/chaotic debris, with superimposed extensive surficial mass wasting processes. In 2019, the rockslide experienced a significant change of behavior and attained exceptional rates of surface displacement, which nevertheless did not develop into sudden movement and large-scale collapse. Hazard assessment is made difficult by the complex nature of the phenomenon, and by the fact that borehole logging and installation of inclinometer casings have long been prevented by the continuing large displacements. More than a decade of GBInSAR data was therefore reviewed to track the remarkable evolution of the slope both in space and time, yielding updated insights into its deformation behavior. In particular, displacement data served as the basis to infer the thickness of the rapidly moving layer of upper chaotic debris downslope of the lower scarp. Activity across the entire rockslide area was also confirmed to be closely and similarly correlated with hydrological forcing. Resulting FEM modelling suggested the existence of a strikingly non-linear vertical velocity profile from slide base up to the surface, modulated by groundwater recharge. The debris cover downslope of the lower scarp was interpreted as being near limit equilibrium even in the absence of external forcing, whereas the onset of movements in the upper scarp area and of the fractured/disturbed substrate at depth as being predominantly governed by abrupt rises of piezometric levels. In spite of the variability of material composition, morphology, and activity, each slope sector appears to share comparable relative trends of surface displacement—and thus the same underlying driving mechanism. The experience gained at Ruinon highlights that the implementation of long-term GBInSAR monitoring may be essential in the case of highly disaggregated and rapidly evolving rockslides that, being subject to recurrent reactivations and associated large displacements, would otherwise be difficult to investigate because of the inaccessibility of the site.

Declaration of Competing Interest

The authors declare that they have no known competing financial interests or personal relationships that could have appeared to influence the work reported in this paper.

Acknowledgements

The GBInSAR system used in this study was designed and produced by Ellegi s.r.l. (a European Commission Joint Research Centre spin-off), which is the holder of proprietary GBInSAR LiSALab technology. Ellegi s.r.l. is acknowledged for collecting and processing the interferometric data. The authors are grateful to ARPA Lombardia for providing the UAV-based terrain point clouds and orthorectified aerial photos that were used for tracking the morphological changes of the slope and

validating the GBInSAR dataset. ARPA Lombardia also collected the weather and piezometric measurements presented in this study. Finally, the authors would like to thank Regione Lombardia and ERSAF (Direzione Parco dello Stelvio) for supporting this study and providing the outcomes of the investigations concerning the characterization of the soil/rock properties at the site.

References

Agliardi, F., Crosta, G., Zanchi, A., 2001. Structural constraints on deep-seated slope deformation kinematics. Eng. Geol. 59, 83–102.
Agliardi, F., Scuderi, M.M., Fusi, N., Collettini, C., 2020. Slow-to-fast transition of giant creeping rockslides modulated by undrained loading in basal shear zones. Nat. Commun. 11, 1352.
Antonello, G., Casagli, N., Farina, P., Leva, D., Nico, G., Sieber, A.J., Tarchi, D., 2004. Ground-based SAR interferometry for monitoring mass movements. Landslides 1, 21–28.
Aryal, A., Brooks, B.A., Reid, M.E., 2015. Landslide subsurface slip geometry inferred from 3-D surface displacement fields. Geophys. Res. Lett. 42, 1411–1417.
Atzeni, C., Barla, M., Pieraccini, M., Antolini, F., 2015. Early warning monitoring of natural and engineered slopes with ground-based synthetic-aperture radar. Rock Mech. Rock. Eng. 48, 235–246.
Barla, G., Antolini, F., Barla, M., Mensi, E., Piovano, G., 2010. Monitoring of the Beauregard landslide (Aosta Valley, Italy) using advanced and conventional techniques. Eng. Geol. 116, 218–235.
Barla, M., Antolini, F., Bertolo, D., Thuegaz, P., D'Aria, D., Amoroso, G., 2017. Remote monitoring of the Comba Citrin landslide using discontinuous GBInSAR campaigns. Eng. Geol. 222, 111–123.
Bishop, K.M., 1999. Determination of translational landslide slip surface depth using balanced cross sections. Environ. Eng. Geosci. 5, 147–156.
Bonzanigo, L., Eberhardt, E., Loew, S., 2007. Long-term investigation of a deep-seated creeping landslide in crystalline rock. Part I. Geological and hydromechanical factors controlling the Campo Vallemaggia landslide. Can. Geotech. J. 44, 1157–1180.
Caduff, R., Schlunegger, F., Kos, A., Wiesmann, A., 2015. A review of terrestrial radar interferometry for measuring surface change in the geosciences. Earth Surf. Process. Landf. 40, 208–228.
Carlà, T., Nolesini, T., Solari, L., Rivolta, C., Dei Cas, L., Casagli, N., 2019. Rockfall forecasting and risk management along a major transportation corridor in the Alps through ground-based radar interferometry. Landslides 16, 1425–1435.
Casagli, N., Catani, F., Del Ventisette, C., Luzi, G., 2010. Monitoring, prediction, and early warning using ground-based radar interferometry. Landslides 7, 291–301.
Crosta, G.B., Agliardi, F., 2003. Failure forecast for large rock slides by surface displacement measurements. Can. Geotech. J. 40, 176–191.
Crosta, G.B., di Prisco, C., Frattini, P., Frigerio, G., Castellanza, R., Agliardi, F., 2014. Chasing a complete understanding of the triggering mechanisms of a large rapidly evolving rockslide. Landslides 11, 747–764.
Crosta, G.B., Agliardi, F., Rivolta, C., Alberti, S., Dei Cas, L., 2017. Long-term evolution and early warning strategies for complex rockslides by real-time monitoring. Landslides 14, 1615–1632.
Cruden, D.M., Varnes, D.J., 1996. Landslide types and processes. In: Turner, A.K., Schuster, R.L. (Eds.), Landslides: Investigation and Mitigation. Transportation Research Board, Washington, pp. 36–75.
Del Ventisette, C., Casagli, N., Fortuny-Guasch, J., Tarchi, D., 2012. Ruinon landslide (Valfurva, Italy) activity in relation to rainfall by means of GBInSAR monitoring. Landslides 9, 497–509.
Duncan, J.M., Wright, S.G., Brandon, T.L., 2014. Soil Strength and Slope Stability, 2nd edition. John Wiley & Sons, Hoboken, New Jersey.
Eberhardt, E., 2008. Twenty-ninth Canadian Geotechnical Colloquim: the role of advanced numerical methods and geotechnical field measurements in understanding complex deep-seated rock slope failure mechanisms. Can. Geotech. J. 45, 484–510.
Eberhardt, E., Stead, D., Coggan, J.S., 2004. Numerical analysis of initiation and progressive failure in natural rock slopes—the 1991 Randa rockslide. Int. J. Rock Mech. Min. Sci. 41, 69–87.
Emery, J.J., 1979. Simulation of slope creep. In: Voight, B. (Ed.), Developments in Geotechnical Engineering. Elsevier, Amsterdam, pp. 669–691.
Glastonbury, J., Fell, R., 2008. Geotechnical characteristics of large slow, very slow, and extremely slow landslides. Can. Geotech. J. 45, 984–1005.
Griffiths, D.V., Lane, P.A., 1999. Slope stability analysis by finite elements. Géotechnique 49, 387–403.
Hungr, O., Corominas, J., Eberhardt, E., 2005. Estimating landslide motion mechanism, travel distance and velocity. In: Hungr, O., Fell, R., Couture, R., Eberhardt, E. (Eds.), Landslide Risk Management. Taylor & Francis Group, London, pp. 99–128.
Hungr, O., Leroueil, S., Picarelli, L., 2014. The Varnes classification of landslide types, an update. Landslides 11, 167–194.
Hutchinson, J.N., 1983. Methods of locating slip surfaces in landslides. Bull. Assoc. Eng. Geol. 20, 235–252.
Infrastrutture Lombarde, 2013. Technical report (in Italian) "Intervento di protezione e valorizzazione dei territori dell'Alta Valtellina attraverso la difesa degli abitati e delle infrastrutture dalla frana del Ruinon di Valfurva (SO) — Modello geotecnico e geomeccanico di riferimento".
Iverson, R.M., 2005. Regulation of landslide motion by dilatancy and pore pressure feedback. J. Geophys. Res. Earth Surf. 110, F02015.
Jaboyedoff, M., Carrea, D., Derron, M.-H., Oppikofer, T., Penna, I.M., Rudaz, B., 2020. A review of methods used to estimate initial landslide failure surface depths and volumes. Eng. Geol. 267, 105478.
Luzi, G., Pieraccini, M., Mecatti, D., Noferini, L., Guidi, G., Moia, F., Atzeni, C., 2004. Ground-based radar interferometry for landslides monitoring: atmospheric and instrumental decorrelation sources on experimental data. IEEE Trans. Geosci. Remote Sens. 42, 2454–2466.
Meier, C., Jaboyedoff, M., Derron, M.-H., Gerber, C., 2020. A method to assess the probability of thickness and volume estimates of small and shallow initial landslide ruptures based on surface area. Landslides 17, 975–982.
Monserrat, O., Crosetto, M., Luzi, G., 2014. A review of ground-based SAR interferometry for deformation measurement. ISPRS J. Photogramm. 93, 40–48.
Palis, E., Lebourg, T., Tric, E., Malet, J.-P., Vidal, M., 2017. Long-term monitoring of a large deep-seated landslide (La Clapiere, South-East French Alps): initial study. Landslides 14, 155–170.
Pieraccini, M., Miccinesi, L., 2019. Ground-based radar interferometry: a bibliographic review. Remote Sens. 11, 1029.
Preisig, G., 2020. Forecasting the long-term activity of deep-seated landslides via groundwater flow and slope stability modelling. Landslides 17, 1693–1702.
Preisig, G., Eberhardt, E., Smithyman, M., Preh, A., Bonzanigo, L., 2016. Hydromechanical rock mass fatigue in deep-seated landslides accompanying seasonal variations in pore pressures. Rock Mech. Rock. Eng. 49, 2333–2351.
Rocscience, 2021. RS2 version 11.009 (computer program). 2D Geotechnical Finite Element Analysis. Available from. https://www.rocscience.com/support/program-downloads (accessed 7 June 2021).
Schulz, W.H., McKenna, J.P., Kibler, J.D., Biavati, G., 2009. Relations between hydrology and velocity of a continuously moving landslide—evidence of pore-pressure feedback regulating landslide motion? Landslides 6, 181–190.
Tarchi, D., Casagli, N., Moretti, S., Leva, D., Sieber, A.J., 2003. Monitoring landslide displacements by using ground-based synthetic aperture radar interferometry: application to the Ruinon landslide in the Italian Alps. J. Geophys. Res. 108, 2387.
Vallet, A., Charlier, J.B., Fabbri, O., Bertrand, C., Carry, N., Mudry, J., 2016. Functioning and precipitation-displacement modelling of rainfall-induced deep-seated landslides subject to creep deformation. Landslides 13, 653–670.
Woods, A., Hendry, M.T., Macciotta, R., Stewart, T., Marsh, J., 2020. GB-InSAR monitoring of vegetated and snow-covered slopes in remote mountainous environments. Landslides 17, 1713–1726.
Zangerl, C., Fey, C., Prager, C., 2019. Deformation characteristics and multi-slab formation of a deep-seated rock slide in a high alpine environment (Bliggspitze, Austria). Bull. Eng. Geol. Environ. 78, 6111–6130.